AD-A198 712 STRENGTH AND MICROSTRUCTURE OF CERAMICS(U) NATIONAL BUREAU OF STANDARDS GAITHERSBURG MD CERAMICS DIV B R LAWN ET AL NOV 87 AFOSR-TR-87-2041 1/1

UNCLASSIFIED AFOSR-ISSA-87-00014 F/G 11/2 NL

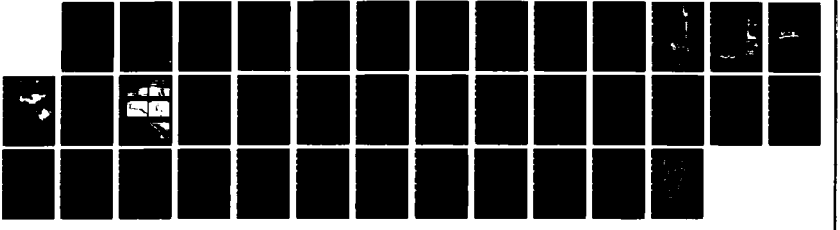

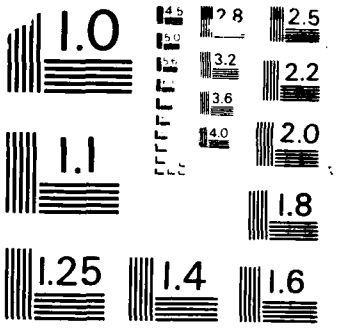

MICROCOPY RESOLUTION TEST CHART
NATIONAL BUREAU OF STANDARDS-1963-A

SECURITY CLASSIFICATION OF THIS PAGE

AD-A190 712

CUMENTATION PAGE

Form Approved
OMB No. 0704-0188

UNCLASSIFIED

1b RESTRICTIVE MARKINGS

DTIC FILE COPY

2a. SECURITY CLASSIFICATION AUTHORITY

3. DISTRIBUTION/AVAILABILITY OF REPORT

Approved for public release,
distribution unlimited

2b. DECLASSIFICATION/DOWNGRADING SCHEDULE

4. PERFORMING ORGANIZATION REPORT NUMBER(S)

5. MONITORING ORGANIZATION REPORT NUMBER(S)

AFOSR-TR- 87-2041

6a. NAME OF PERFORMING ORGANIZATION
NATIONAL BUREAU OF STANDARD

6b. OFFICE SYMBOL (If applicable)

7a. NAME OF MONITORING ORGANIZATION
AFOSR/NE

6c. ADDRESS (City, State, and ZIP Code)
GAITHERSBURG, MD 20899

7b. ADDRESS (City, State, and ZIP Code)
BLDG 410
BOLLING AFB, DC 20332-6448

8a. NAME OF FUNDING/SPONSORING ORGANIZATION
AFOSR/NE

8b. OFFICE SYMBOL (If applicable)

9. PROCUREMENT INSTRUMENT IDENTIFICATION NUMBER
AFOSR-ISSA-87-0034

8c. ADDRESS (City, State, and ZIP Code)
BLDG 410
BOLLING AFB, DC 20332-6448

10. SOURCE OF FUNDING NUMBERS

PROGRAM ELEMENT NO.	PROJECT NO.	TASK NO	WORK UNIT ACCESSION NO.
61102F	2306	A2	

11. TITLE (Include Security Classification)
STRENGTH AND MICROSTRUCTURE OF CERAMICS

12. PERSONAL AUTHOR(S)
Lawn

13a. TYPE OF REPORT	13b. TIME COVERED	14. DATE OF REPORT (Year, Month, Day)	15. PAGE COUNT
ANNUAL REPORT	FROM 01/10/86 TO 30/09/87		

16. SUPPLEMENTARY NOTATION

17. COSATI CODES			18. SUBJECT TERMS (Continue on reverse if necessary and identify by block number)
FIELD	GROUP	SUB-GROUP	

19. ABSTRACT (Continue on reverse if necessary and identify by block number)

Our goal in this program continues to be the understanding of the role of microstructure in the strength properties of ceramics. It is becomming increasingly apparent to the brittle fracture community that the toughness characteristics and flaw distributions of structural ceramics can be very much influenced, sometimes with great sensitivity, by small details in the microstructural makeup. For instance, the addition of less than 1% glassy phase to the grain boundaries of alumina polycrystals can alter the fracture properties dramatically, giving rise to significant improvements in strength.

DTIC
ELECTE
JAN 19 1988
S E

20 DISTRIBUTION/AVAILABILITY OF ABSTRACT
☐ UNCLASSIFIED/UNLIMITED ☐ SAME AS RPT. ☐ DTIC USERS

21. ABSTRACT SECURITY CLASSIFICATION
UNCLASSIFIED

22a. NAME OF RESPONSIBLE INDIVIDUAL	22b. TELEPHONE (Include Area Code)	22c. OFFICE SYMBOL
ROSENSTEIN	(202) 767-4933	NE

DD Form 1473, JUN 86 Previous editions are obsolete. SECURITY CLASSIFICATION OF THIS PAGE

AFOSR-TR- 87-2041

STRENGTH AND MICROSTRUCTURE OF CERAMICS

Brian R. Lawn

(and R.F. Cook, C.J. Fairbanks, B.J. Hockey, Y-W Mai,
P.L. Swanson, D.B. Marshall)

Technical Report

AFOSR Contract No. ISSA-87-0034
NBS Project No. 4200464

for

Air Force Office of Scientific Research
Bolling Air Force Base
Washington, DC 20332

by

Ceramics Division
National Bureau of Standards
Gaithersburg, MD 20899

November 1987

88

STRENGTH AND MICROSTRUCTURE OF CERAMICS

Accession For
NTIS GRA&I ☒
DTIC TAB ☐
Unannounced ☐
Justification
By
Distribution/
Availability Codes
Dist | Avail and/or Special
A-1

DTIC COPY INSPECTED 6

INTRODUCTION

Our goal in this program continues to be the understanding of the role of microstructure in the strength properties of ceramics. It is becoming increasingly apparent to the brittle fracture community that the toughness characteristics and flaw distributions of structural ceramics can be very much influenced, sometimes with great sensitivity, by small details in the microstructural makeup. For instance, the addition of less than 1% glassy phase to the grain boundaries of alumina polycrystals can alter the fracture properties dramatically, giving rise to significant improvements in strength. However, without the additive phase the material is found to have the highly desirable quality of "flaw tolerance", i.e. an insensitivity of the strength to the initial crack size. It becomes important to understand such subtle interrelations between materials characterization and fracture processes, in order that we may on the one hand be able to establish reliable design criteria and, on the other, tailor new, superior ceramics.

Emphasis is being placed on characterization of the grain boundary interface in "model" ceramic systems, such as polycrystalline Al_2O_3, so that the mechanical properties can be closely related to controllable processing variables (e.g. impurity content, grain size, etc.). The toughness response, particularly the R-curve (crack resistance curve as function of crack size), is being followed as a function of these variables. It is expected that new insights will be gained into the role of interfacial phenomena in mechanical behavior, insights that will ultimately bear on such practical areas as composite fabrication, coating-substrate technology, etc. The proposed research offers a systematic approach to the design and tailoring of new structural ceramic materials.

To this end, NBS has established a joint venture with the ceramic processing group, under the direction of Dr. M.P. Harmer, at Lehigh University. AFOSR has committed funds to Dr. Harmer's group as part of a companion, collaborative processing-tailoring (Lehigh) and mechanical evaluation (NBS) program.

During the past year, work has focussed on the elaboration of the R-curve behavior in alumina ceramics. This work is summarized in the four appended papers:

(1) Paper 1 describes an in-situ study of crack propagation in alumina. The predominant toughening mechanism is that of "grain bridging". The observations show that interlocking grains and ligaments of unbroken material in the wake of the crack front serve to apply closure forces to the crack surfaces: these forces must be overcome for the crack to propagate. This is a radical new observation, which has not been considered in any previous theory of toughening.

(2) Paper 2 describes a theoretical fracture mechanics model of grain-localized ligament restraint behind an advancing crack tip. This model was developed in collaboration with Dr. Y.W. Mai, Guest Worker from the University of Sydney. The theory provides a full fit of the R-curve for various aluminas and glass ceramics. The one missing element in this analysis was the underlying physical mechanism by which the interlocking grain bridges were set up. We now believe that the restraint is tied up with "locked-in" thermal expansion mismatch stresses in the non-cubic alumina structure. We are currently incorporating this element into our theoretical analysis.

(3) Paper 3 takes the theory from papers 1 and 2 and uses it to determine the strength characteristics of ceramics. We have been able to use

the ensuing formulations to extract the fundamental toughness crack-size dependencies for various aluminas and other ceramics, using a computer best-fitting algorithm. We are currently fabricating alumina ceramics to enable us to investigate the role of critical microstructural variables on the strength behavior more closely. In particular, we are seeking conditions which optimize the quality of "flaw tolerance" which is associated with strong R-curve behavior.

(4) Paper 4 describes experimental grinding resistance data, and relates these data to the R-curves. It is found, contrary to conventional wisdom, that large-scale macroscopic toughness does not correlate with grinding resistance. This is a consequence of teh R-curve behavior. Consequently, the R-curve must be considered when selecting ceramic materials for optimum wear resistance.

Reprinted from the Journal of the American Ceramic Society, Vol. 70, No. 4, April 1987
Copyright 1987 by The American Ceramic Society

Crack-Interface Grain Bridging as a Fracture Resistance Mechanism in Ceramics: I, Experimental Study on Alumina

PETER L. SWANSON,* CAROLYN J. FAIRBANKS, BRIAN R. LAWN,* YIU-WING MAI,* and BERNARD J. HOCKEY

Ceramics Division, National Bureau of Standards, Gaithersburg, Maryland 20899

Direct microscopic evidence is presented in support of an explanation of *R*-curve behavior in monophase ceramics by grain-localized bridging across the newly formed crack interface. In situ observations are made of crack growth in tapered cantilever beam and indented flexure specimens of a coarse-grained alumina. The fractures are observed to be highly stable, typical of a material with a strongly increasing resistance characteristic, but are *discontinuous* at the microstructural level. Associated with this discontinuity is the appearance of overlapping segments in the surface fracture trace around bridging grains; the mean spacing of such "activity sites" along the trace is about 2 to 5 grain diameters. These segments link up with the primary crack beneath the specimen surface, and continue to evolve toward rupture of the bridge as fracture proceeds. The bridges remain active at large distances, of order 100 grain diameters or more, behind the crack tip. Scanning electron microscopy of some of the bridging sites demonstrates that secondary (interface-adjacent) microfracture and frictional tractions are important elements in the bridge separation process. Evidence is sought, but none found, for some of the more popular alternative models of toughening, notably frontal-zone microcracking and crack-tip/internal-stress interaction. It is suggested that the crack-interface bridging mechanism may be a general phenomenon in nontransforming ceramics.

I. Introduction

THERE is a growing realization that the crack resistance properties of ceramics have an intrinsic size dependence.[1] At crack sizes small in relation to the microstructure the toughness has values characteristic of bulk cleavage (transgranular) or grain boundary (intergranular) energies. At large crack sizes the toughness tends to somewhat higher, limiting values characteristic of the polycrystalline aggregate. The toughness function connecting these two extremes in crack size is the so-called "*R*-curve" function, after the rising crack resistance curves originally found for metals.[2] Such *R*-curve behavior is of great interest in the case of engineering ceramics, for both the structural designer, who needs to know the toughness characteristic in specifiable flaw size ranges, and the materials processor, who seeks a basis for tailoring new and superior materials.

Despite this increasing awareness of the importance of microstructurally related size effects, there have been remarkably few attempts at definitive identification of underlying crack resistance mechanisms. A notable exception is in the zirconia-based ceramics, where transformation toughening is now unequivocally established as a principal factor.[3-5] The transformation events are generally taken to be confined within a "process zone" about the advancing crack tip, in analogy to the plastic zone responsible for the *R*-curve behavior of metals. However, important as it is as a mode of crack impedance, transformation toughening is currently restricted to a select few ceramics and does not operate in "simple" monophase materials like aluminas. Crack size effects in these latter materials have been attributed to several alternative causes, with virtually no direct experimental substantiation. Perhaps the most widely quoted of these is the proposal of a frontal *microcrack* cloud, in which discrete microfractures act as effective energy sinks in the field of the primary crack.[6,7] Another proposal is that an advancing crack tip is progressively impeded via direct interactions with locked-in internal stresses (e.g., thermal expansion mismatch stresses).[8] Other possibilities that have been considered include crack restraint by pinning and bowing[9] and by deflection and twisting,[10] although these are noncumulative mechanisms; they do not have provision to account for the remarkably long crack size range over which the *R* curve rises in many materials.[1]

Which of the above mechanisms, if any, predominates in the *R*-curve behavior of aluminas and other nontransforming ceramics? The current literature relating to this question is based almost exclusively on the capacity of theoretical models to match measured fracture mechanics (e.g., applied load vs crack size) data. The question of whether or not the proposed mechanisms actually operate in the assumed fashion is not directly addressed in this literature; support is provided only by circumstantial evidence from limited postfailure examinations of fracture specimens. However, there is one set of observations, by Knehans and Steinbrech,[11] which allows us to narrow down the possibilities. They grew cracks through several millimeters in alumina test specimens, and found strong rising *R* curves. Then they removed material adjacent to the walls *behind* the crack tip by sawcutting, taking care to leave intact the immediate region *at* the tip. On restarting the crack, the resistance reverted immediately to the base of the *R* curve. The unmistakable implication was that the toughening processes must operate in the wake of the advancing tip. Of the mechanisms considered thus far, it is that of distributed microcracking which is most compatible with this notion of a wake effect; indeed, the Knehans and Steinbrech experiment has been cited as evidence for the microcracking model.[7]

However, Knehans and Steinbrech raised another possibility, that the source of the rising resistance may lie in some physically restraining force across the newly formed crack interface. This alternative proposal had received only passing mention in the preceding ceramics literature.[12,13] Knehans and Steinbrech have since taken their case further, arguing specifically in favor of a grain interlocking mechanism.[14,15] The idea of an interfacial restraint is not the exclusive domain of the ceramics community; it has been developed even more strongly in concrete[16,17] and rock mechanics,[18,19] although the detailed micromechanics of the actual separation processes are hardly better understood. Thus it would seem that the key to improving the toughness of nontransforming ceramics could depend primarily on events which occur behind rather than at or ahead of the advancing crack. Clearly there are important implications here in the microstructural design of ceramic materials.

The present work is directed to the development of a crack resistance model incorporating the essential elements of the inter-

Presented at the 88th Annual Meeting of the American Ceramic Society, Chicago, IL, April 30, 1986 (Basic Science Division, Paper No. 166-B-86). Received April 16, 1986; revised copy received September 2, 1986; approved October 14, 1986.

Supported by the U.S. Air Force Office of Scientific Research; support for P. L. S. provided by an NRC Postdoctoral Fellowship and support for Y. W. M. provided by the NBS Guest Worker Program.

*Member, the American Ceramic Society.

†On leave from the Department of Mechanical Engineering, University of Sydney, N.S.W. 2006, Australia.

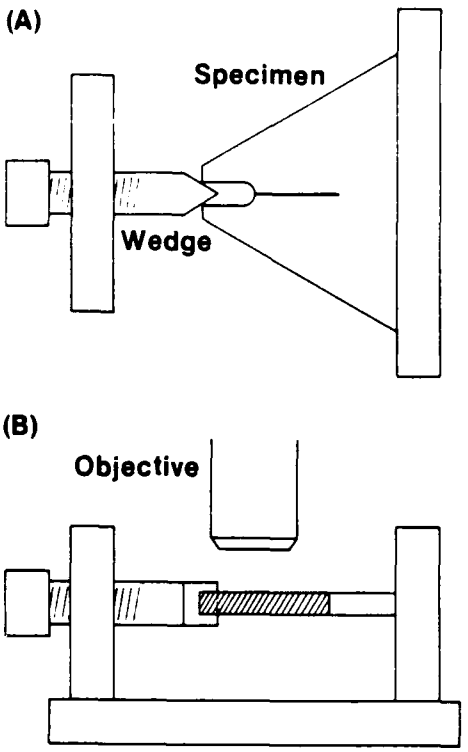

Fig. 1. Schematic of tapered double cantilever beam test specimen used to observe crack growth during loading: (*A*) top view; (*B*) side view. Specimen cut from triangular slab, 12-mm edge length and 2-mm thickness, to produce crack 7 mm long. Starter notch length 300 μm, radius 100 μm. Wedge angle 60°.

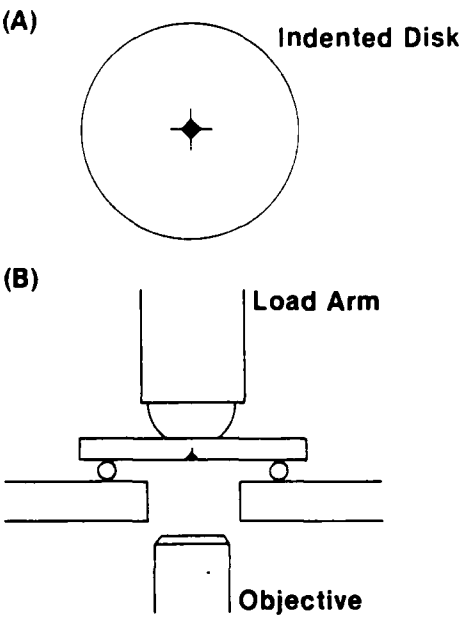

Fig. 2. Schematic of indentation flaw test used to observe radial crack evolution to failure: (*A*) plan view, showing Vickers flaw on tensile surface; (*B*) side view, showing flexure system. Specimen dimensions 25-mm diameter by 2-mm thickness. Biaxial loading, 2-mm-radius punch on 10-mm-radius (3-point) support.

facial restraint concept. It is in two parts. Part I describes experimental observations of controlled crack growth in a coarse-grained alumina with strong *R*-curve behavior. A critical feature of these experiments is the facility to follow the crack response along its entire length while the driving force is being applied. We confirm the presence of grain-localized "bridges" across the crack interface, over large distances (several millimeters) behind the tip. Part II deals with quantitative aspects of the *R*-curve behavior, by a formulation of the bridging concept in terms of theoretical fracture mechanics. In this endeavor we borrow from analogous treatments in the fiber-reinforced composite and concrete literature. Our analysis does not aspire to a complete understanding of the physical ligamentary rupture process, but nevertheless establishes a sound mechanical framework for characterizing the crack resistance properties.

Before proceeding, it is well that we should draw attention to a recent study on the strength properties of ceramic specimens containing indentation flaws.[20-22] Indeed, some of the issues raised in that study provided a strong motivation for the present work. There, the idea was to investigate the fracture size range between the extremes of the microscopic flaw and the macroscopic crack by systematically varying the indentation load from specimen to specimen. It was found that on reducing the indentation flaw size the corresponding strength did not increase indefinitely, as required by ideal indentation fracture theory (i.e., theory based on the notion of an invariant toughness), but tended instead to level off at a strength characteristic of the intrinsic microstructural flaws. This response was attributed to the influence of *R*-curve behavior. Importantly, the strength plateau at small flaw sizes was seen in three groups of ceramics, aluminas, glass-ceramics, and barium titanates, indicating a certain generality in the *R*-curve phenomenon. Also, the magnitude of the effect was in some cases considerable, amounting to an effective increase in toughness of more than a factor of 3 over a crack size range of some tens of grain sizes or more. In that earlier study[20] the microstructural element was introduced into the fracture mechanics in a somewhat phenomenological manner: here we seek to place the fracture mechanics on a firmer footing by relating this element more closely to identifiable crack restraint mechanisms. Accordingly, a detailed analysis of indentation fracture data in terms of the bridging concept may be foreshadowed as a future goal of our work.[23]

II. Experimental Procedure

It was decided in this work to focus on one material, a nominally pure, coarse-grained alumina.[†] We have already made allusion to the implied generality of the *R*-curve phenomenon (Section I); our choice is intended to meet the requirement of a "representative" material, but at the same time one which exhibits the *R* curve to particularly strong effect. (For quantitative measures of the pertinent *R* curve the reader is directed to the "M"-labeled curves in Figs. 4 and 10 in Ref. 20, Figs. 6 and 7 in Ref. 1, and Figs. 1 and 3 in Ref. 22.) The relatively large microstructure of our material (mean grain diameter 20 μm) also lends itself to in situ experimentation using ordinary means of microscopic observation. In certain instances where it was deemed useful to run comparative tests on specimens *without* the influence of microstructure, sapphire was used as a control material.

As indicated, a major feature of our experimental procedure is the facility to monitor the evolution of fracture during the application of stress. Accordingly, direct observations were made of the crack growth by optical microscopy, using the two loading configurations shown in Figs. 1 and 2. The specimens were surface-relief polished with 0.3-μm Al_2O_3 powder to delineate the coarser grain boundary structure. In some cases a thermal etch pretreatment at (1050°C for 2 h) was used to enhance fine details in

[†]Vistal grade, Coors Porcelain Co., Golden, CO.

this structure. An important element of our experimental philosophy here is that, by virtue of the enhanced stabilization in crack growth which attends strong *R*-curve behavior,[1] we may hope to observe critical events which in conventional postfailure analysis (or even in interrupted tests) might pass unnoticed.

The first of the test configurations, Fig. 1, is a modification of the familiar double cantilever beam specimen. Generally, the regular rectangular beam geometry is retained for *quant*itative evaluation of the *R*-curve behavior (Part II). Here, however, a tapered geometry was used, width increasing in the direction of ultimate crack propagation. The main crack was started at a sawcut notch by inserting a metal wedge. Subsequent crack extension could be controlled via a micrometer drive system, to which the wedge was fixed. The whole system was attached to the stage of an optical microscope to allow for continuous monitoring of the crack evolution. Pertinent dimensions of the test geometry are included in the caption to Fig. 1.

The second configuration, Fig. 2, simulates the controlled flaw test used previously to infer *R*-curve behavior from strength data (Section I). A Vickers diamond was used to introduce an indentation flaw at the center of a disk flexure specimen. The disk was then loaded axially in a circular-flat on three-ball-support fixture,[24] with the indentation on the tension side. Again, the entire fixture was attached to a microscope stage for in situ viewing of the crack evolution. A video recording unit was particularly useful in interpreting some of the more subtle features observed with this configuration. Reference is made to Fig. 2 for relevant test geometry dimensions.

Some additional, static observations were made on the above specimens to add weight to our ensuing case. For example, in the event of toughening associated with a frontal microcrack cloud, one might anticipate some detectable surface distortion either ahead or in the wake of the primary crack tip. Accordingly, surface profilometry scans were taken perpendicular to the crack traces on some of the cantilever specimens. The cantilever configuration was more convenient in this regard because the entire wedge-loading fixture could be transferred onto the profilometer stage, thereby allowing the crack to be examined without unloading. Also, anticipating that we might need to look more closely at events at the level of the grain size *or below*, some of the unloaded disk specimens were examined by scanning electron microscopy.

III. Results

(1) General Observations

Our initial examinations of the fracture patterns produced in the alumina test specimens revealed some interesting general features. The clearest and most immediate indication that we were dealing with a crack-interface effect was that, after "failure" (as marked by a sudden propagation of the cracks to the edges of the specimen), the fractured segments tended to remain intact. An additional force was required to separate the pieces completely. This was our first clue that the walls behind an advancing tip must indeed be restrained by some remnant forces acting across the interface.

Closer surface inspections along the crack traces at various stages of propagation soon helped to reinforce this last conviction. The fracture in our material was predominantly intergranular, as previously reported.[20,21] There were signs of some "secondary activity" adjacent to the walls of the otherwise primary crack interface, but never further distant than one or two grain diameters from this interface. It will be our aim in the following sections to confirm that this interface-related activity is a manifestation of a grain-localized ligamentary rupture process, and not of some relaxation effect associated with the wake of an advancing microcrack cloud.

Interfacial tractions and bridging by as-yet-unruptured grains may *independently* provide tractions across the nascent fracture surface. Distinction between these two potential sources of tractions is not a principal concern here, owing to the experimental difficulties in resolving finer details in the subsurface damage processes.[1,2]

(2) Cantilever Beam Experiments

The in situ observations of fracture in the tapered cantilever beam specimens (Fig. 1) were carried out while carefully and slowly driving in the mouth-opening wedge. These observations were all made in air, so that some rate effects were apparent in the crack growth (although the velocities were usually much less than 10^{-5} m·s^{-1}). There was a tendency for the first stage of fracture to occur suddenly over a distance of several grain diameters from the starter notch tip. "Pop-in" behavior of this kind is not uncommon in notched specimens, of course; in such cases the initial fracture response can be influenced strongly by the local notch configuration. However, discontinuous crack growth was also commonly observed in the subsequent loading, over distances as small as one or two grains. There is the suggestion here of an element of discreteness in the mechanics which ultimately underlies the *R*-curve behavior.

Appropriately, attention was focused on regions of identifiable "activity sites" behind the advancing crack tip during monotonic loading to "failure." An example of the kind of observation made is shown in Fig. 3, a low-magnification reflected-light mosaic of a particular specimen at six successive stages of fracture. The field of view along the crack length covers the first 2 mm from the starter notch at left (not included in the figure). At final loading, stage VI in Fig. 3, the crack extends clearly across the full 7-mm length of the specimen, although again without separating into two parts. The areas labeled (*A*), (*B*), and (*C*) illustrate particularly clear examples of progressive crack-flank damage evolution through the loading sequence. These areas are magnified in Figs. 4 to 6 for closer scrutiny of the microstructural detail.

In zone *A*, Fig. 4, we can follow the formation and rupture of a single ligamentary bridge through all six stages. In stage I the surface fracture trace appears to be segmented about a large grain, as though the primary crack may have stopped and then reinitiated on a secondary front. However, on switching to transmitted light (e.g., see Fig. 7(*B*)) and focusing into the subsurface regions of the transparent material, the apparently isolated segments were found to connect together into a common crack interface. Hence the bridge is grain-localized in the projected fracture plane. On proceeding to stage II we note that the crack segments about the bridging grain have increased their overlap but have not yet linked up, although the detectable main tip is now some 0.75 mm distant. There is an indication of enhanced reflectivity beneath this same grain, indicating that the crack-segment overlap extends *beneath* as well as *along* the surface. By the time the primary tip has advanced more than 1.2 mm beyond the bridge, stage III, the upper crack segment appears to have linked up completely with the main fracture trace. This does not signify the final state of rupture, however, for there are signs of continued local crack activity around the grain of interest, notably at left, through stages IV and V. We point out that the primary crack tip is at least 2 mm, i.e., approaching 100 grain diameters, ahead of the bridge site. Finally, at stage VI, the lower crack associated with the original bridge appears to have closed up somewhat, perhaps reflecting the release of some interfacial frictional tractions.[1]

Zone *B*, in Fig. 5, evolves in much the same way, but with certain of the above-mentioned features delineated more strongly. The initial crack segmentation, stage III, and subsequent linkup, stage IV, differ little in essence from that observed in zone *A*. However, the trace of the crack segment which runs *below* the bridging grain (and which, incidentally, would appear in stage III to be the more likely to lead to the ultimate rupture of the ligament) closes up much more abruptly and completely than its counterpart in zone *A*. Interfacial tractions persist on loading to stage V, as evidenced by the appearance of additional small-scale fissures about the separating grain. Examination in transmitted light during this stage revealed substantial subsurface activity. Even more dramatic indications of unrelieved tractions are evident from the postmortem configuration at stage VI. Final separation has occurred through virgin material, seemingly "avoiding" the incipient fracture paths apparent in the previous micrographs, a measure of the disruption caused by this final rupture is given by the extensive debris, visible as the region of highly diffuse reflection, lodged

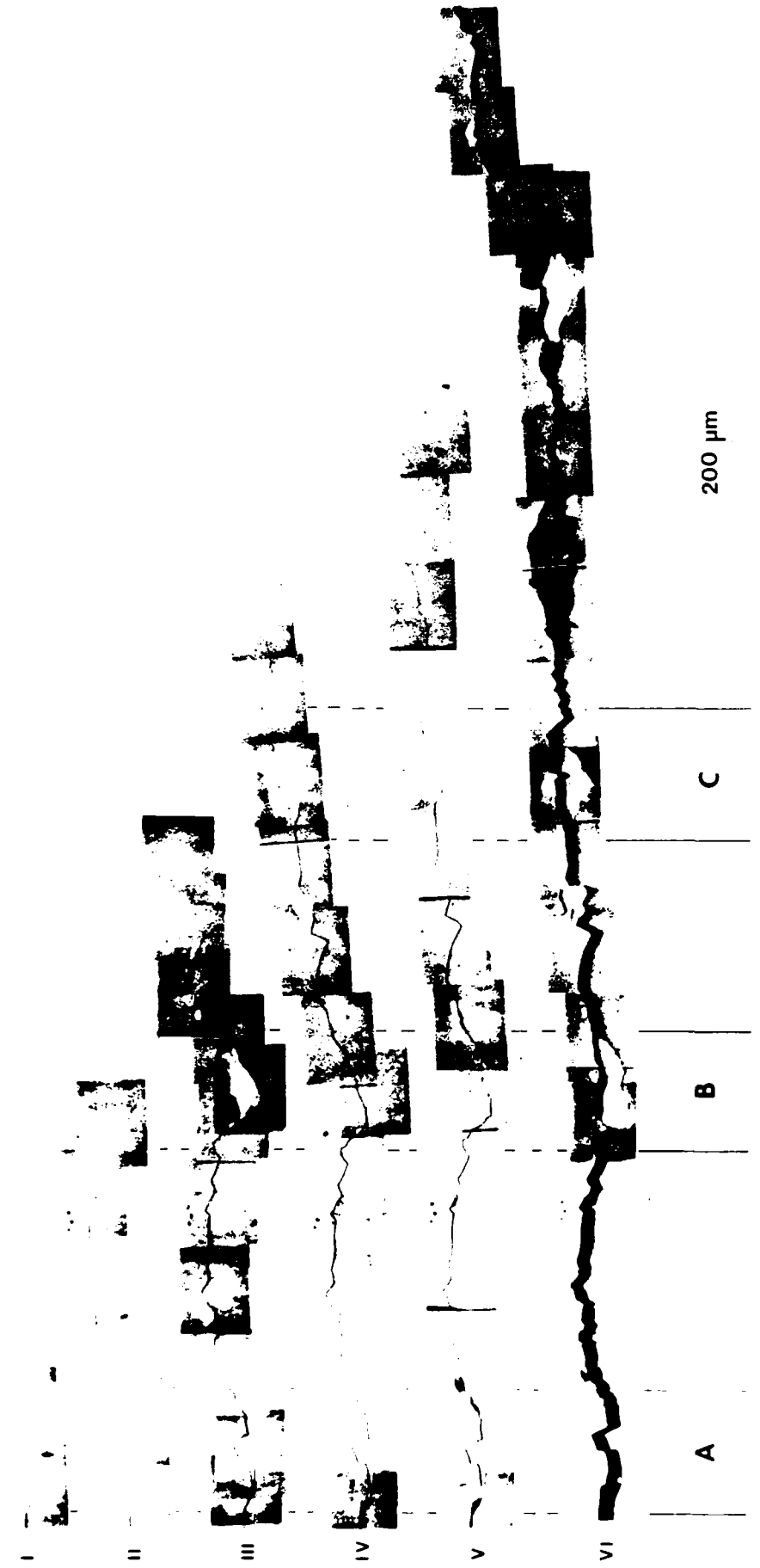

Fig. 3. Reflected light micrograph mosaic of crack evolution in tapered DCB specimen of alumina, shown at six stages of loading. Wedge remains inserted in notch (just out of field at left) in all stages.

Fig. 4. Enlargement of zone *A* in Fig. 3 showing evolution of a grain bridging site from inception to failure. Persistence of interface-related secondary cracking is apparent through stage V.

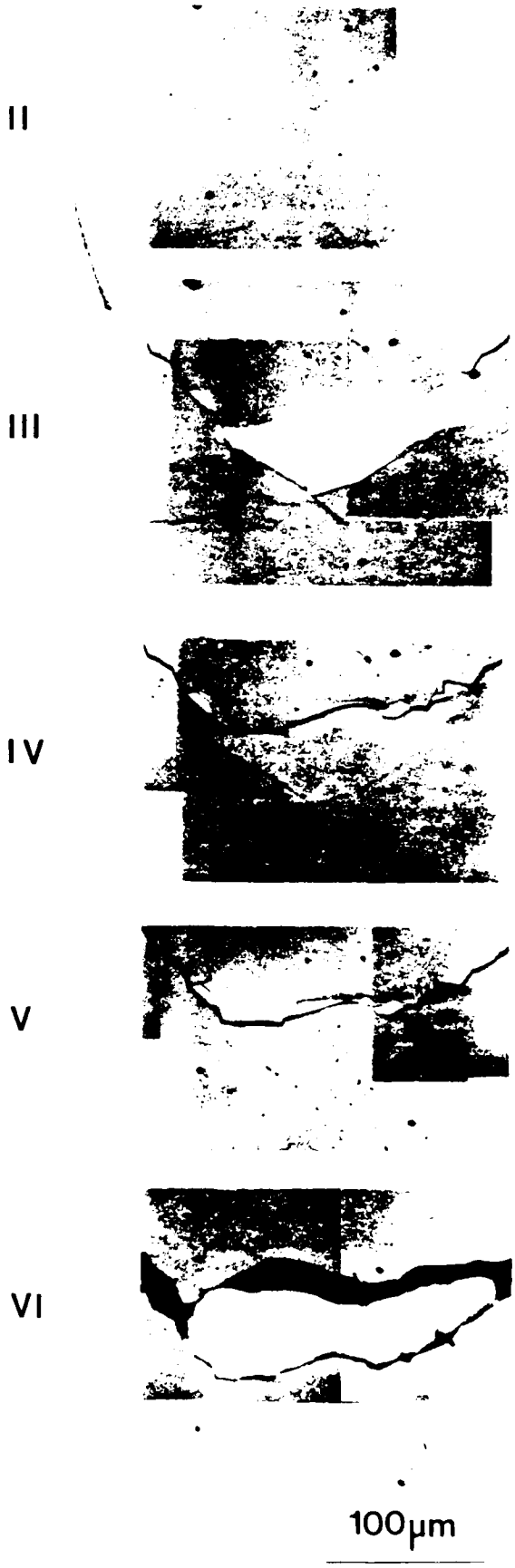

Fig. 5. Enlargement of zone *B* in Fig. 3. Note continually changing course of the local fracture path through the loading to failure.

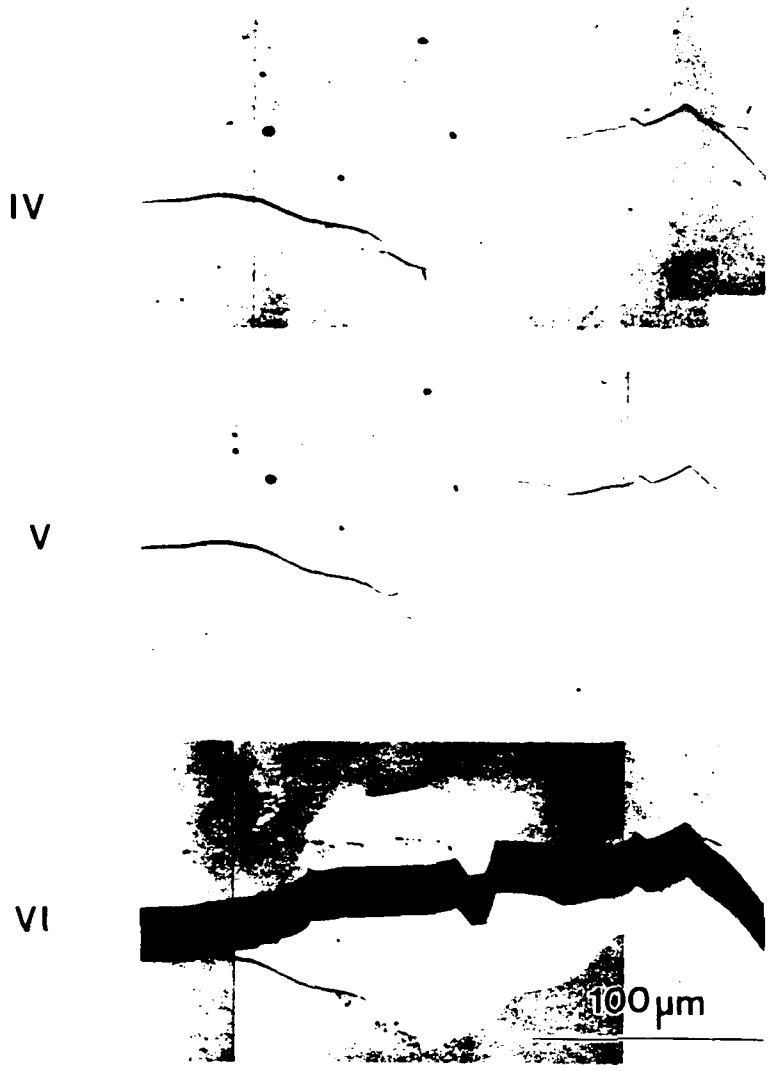

Fig. 6. Enlargement of zone *C* in Fig. 3. Substantial transgranular fracture accompanies the bridge rupture.

between the crack walls at the original bridge site.

Consider now the third area in Fig. 6, zone *C*. In the initial stage, IV, substantial microcrack overlap occurs, predominantly along grain boundaries, followed by transgranular microrupture *within* the initial span of bridging material, stage V. Again, the final rupture path largely ignores the previously formed, localized crack segments.

We note that at each bridge-rupture site (zones *A*, *B*, *C*) the cumulative amount of surface-exposed crack length is approximately *3 times* the shortest straight-line path through the bridging sites. Moreover, the total fracture surface area incorporates a significant amount of transgranular fracturing. The bridges clearly represent an intrinsically high-energy source of fracture resistance.

In choosing our examples above we have, for obvious reasons, focused on the most conspicuous sites, i.e., the sites involving the largest bridging grains. Higher magnification examinations of loaded crack systems such as that in Figs. 3 to 6 revealed a high density of smaller, but no less active, sites, particularly toward the fracture terminus. These were again evident as surface offset traces in reflection or subsurface scattering centers in transmission. It was thereby estimated that the mean separation between grain ligaments could be as low as 2 to 5 grain diameters.

With the realization that our microscopic observations were capable of detecting grain-scale microfractures while load was maintained, particularly in illumination by transmitted light, attention was turned to the region *ahead* of the primary crack terminus. Figure 7 shows typical micrographs of this region. In particular, evidence was sought which might point to the existence of a cloud of distributed microcracks about the terminus. In keeping with the popular notion of discrete microfracture initiation at or above some critical tensile stress level within the near crack field, we might expect to observe diffuse scattering within an extensive frontal microcrack zone.[5,7] No such extended diffuse scattering was ever detected in our experiments. Sometimes apparently unconnected surface traces were observed in the terminus region (e.g., as in Fig. 7(*B*)) but, like their segmented counterparts *behind* the tip, these invariably connected up at a depth of a grain diameter or so beneath the surface.

Further null evidence for an extended transverse microcracking zone was provided by the surface profilometer traces. These were taken perpendicular to the loaded crack configuration seen in stage IV, Fig. 3. The results of several scans, both ahead and behind the crack tip, are shown in Fig. 8. Minute surface detail associated with the relief polishing is apparent in the scans, but in no case is there any indication of a general dilation-induced uprising of material adjacent to the crack interface.

(3) *Indentation-Strength Experiments*

Direct observations were made of crack growth from Vickers indentation flaws during loading to failure (Fig. 2). An example of the final fracture pattern produced in this configuration is given in Fig. 9. We see that once the initial radial cracks traverse the central

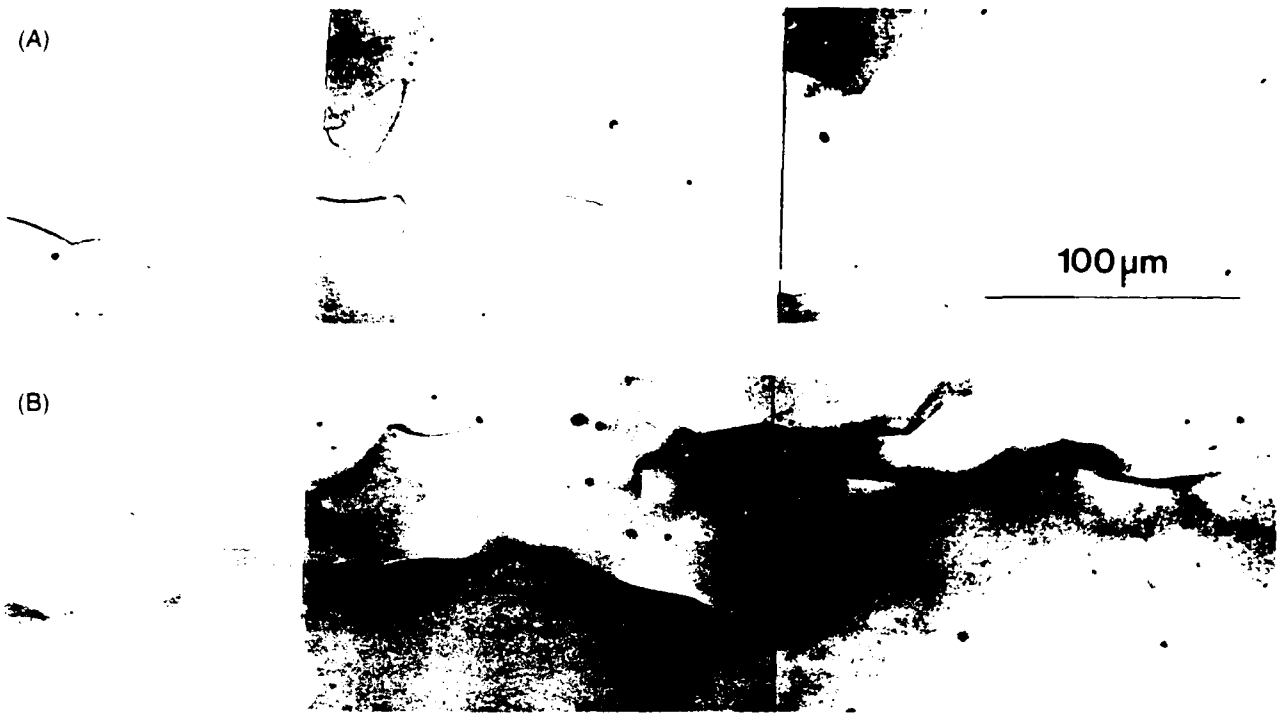

Fig. 7. Reflection (*A*) and transmission (*B*) micrographs of loaded DCB specimen (equivalent in growth to about stage IV in Fig. 3).

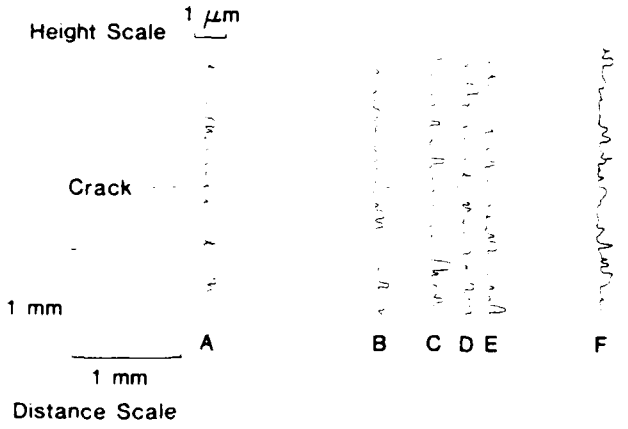

Fig. 8. *Surface profilometer traces transverse to crack plane in loaded* alumina DCB specimen. Detectable crack tip lies on trace *D*. Height scale on scan greatly magnified relative to distance scale. No surface uplift adjacent to crack walls is evident (diamond stylus radius ≈1 μm, horizontal position uncertainty ±100 μm, vertical uncertainty <10 nm for long wavelength, i.e., ≥10 μm, topography variations).

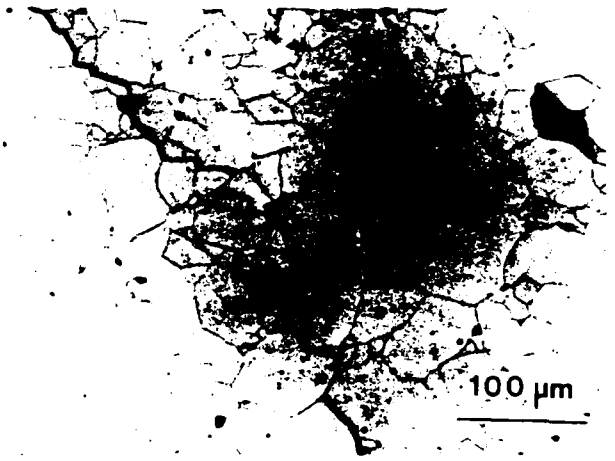

Fig. 9. Reflected light micrograph of a Vickers indentation site in a "fractured" alumina disk. Initial radial cracks from low-load (5 N) indentation arrest at first encounter with grain boundary, and grow discontinuously *along* boundaries as flexural stress is applied. Specimen thermally etched to reveal grain structure.

grains which encompass the indentation impression, the fracture proceeds primarily in the familiar intergranular mode. Once more, this fracture runs to the specimen extremities without causing complete separation.

One of our acknowledged goals here was to look in fine detail at the crack response *prior to* failure. Accordingly, the tests were run at slow stressing rates, in air, for greatest ease of observation. *Typically, the time to failure was several minutes.* At high indentation loads (≥100 N), such that the scale of the starting radial cracks substantially exceeded that of the microstructure, the fracture showed an even stronger tendency to discontinuous evolution, over distances of a few grains or so, than noted in the cantilever beam experiments. Notwithstanding these discontinuities, the cracks were characterized by strong prefailure stability, sometimes extending to the edges of the 12.5-mm-radius disks without any sign of catastrophic growth. There is no doubt that local residual contact stresses contribute to this stability,[26] but only in part; comparative runs on sapphire (microstructure-free) specimens under identical test conditions show much smaller, i.e., ≪1 mm, precursor stable growth prior to failure. It seems reasonable to conclude that the enhanced stabilization in the polycrystalline alumina is a direct manifestation of a rising R curve.[1]

At low indentation loads (1 to 10 N) the evidence for discontinuity in the stabilized crack growth was even more emphatic

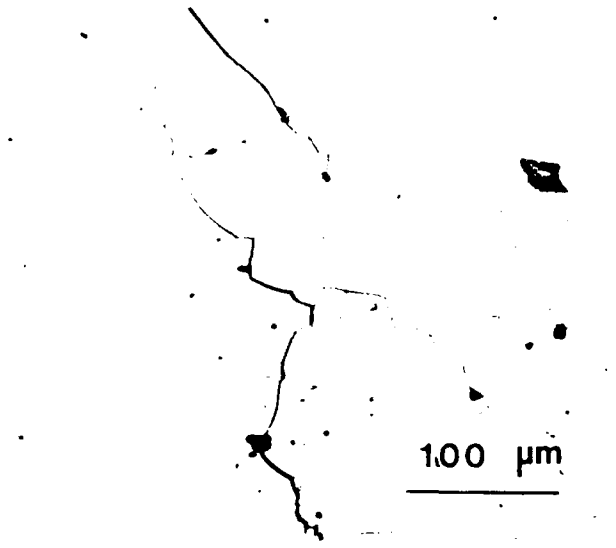

Fig. 10. Reflected light micrograph of a segmented radial crack in a partially fractured alumina disk.

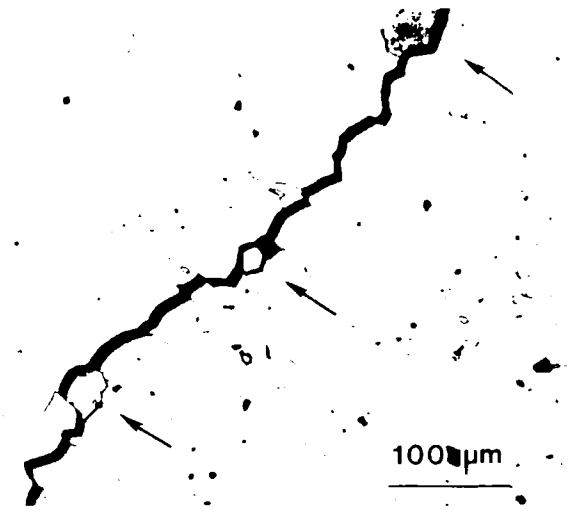

Fig. 11. Reflected light micrograph of portion of a radial crack in a fractured-but-intact alumina disk. Disturbance of some interface-adjacent grains is evident (arrows).

This is the region of the load-insensitive plateau in the strength data[2] referred to in Section I. The radial cracks seemed to remain "trapped" at the encompassing grain boundaries (see Fig. 9) during the flexural loading up to some critical level, at which point a sudden burst of growth ensued. This initial growth pattern was highly variable from specimen to specimen. In many cases the growth distance was small, of the order of grain dimensions, before arresting. Also, individual radial cracks tended to propagate independently, at different levels in the loading. We may liken this initial phase of the fracture evolution to the pop-in observed in the beam configuration (Section II(2)); however, now we can be certain that we are indeed observing an intrinsic property of the small-scale flaw and not some artifact due to the fracture (e.g., notch) geometry. On increasing the applied loading further these radial cracks continued to extend intermittently, but at an increasing jump frequency with respect to stress increment. Thus the "smoothness" in the approach to ultimate failure depended on the number of jumps activated during the loading. In some extreme cases the initial burst of crack propagation was so "energetic" as to take the stressed system spontaneously to failure.

It was also observed that the same kind of discontinuous crack growth and arrest occurred at prominent *natural* flaws in the alumina specimens. These flaws included grain pullout sites on imperfectly polished surfaces and internal fabrication pores. Occasionally such flaws provided the ultimate center of failure, most notably at the low end of the indentation load scale. There seemed little tendency for these competing sites to interact with each other, although inevitably neighbors would occasionally combine to produce an enlarged, yet still stable, composite crack.

Our observations of strong discontinuity and enhanced stabilization in the indentation-strength specimens turns our attention, as in the cantilever beam experiments, to events behind the growing crack tip. Essentially, our in situ examinations of the radial crack evolution to failure revealed the same kind of general grain-bridging features as described earlier in Figs. 4 to 6. Figure 10 shows an example of a particularly large bridging site behind the tip of an extended radial crack. Sites of this kind located as far back as the indentation impression corners remained active throughout the growth to failure, even in those specimens with millimeter-scale stable extensions, confirming that interface restraints act over distances on the order of 100 grains or more. The self-consistency of the grain separation patterns in the two specimen types examined here serves to allay any concern that we might be observing some test-geometry-specific artifact (although geometry effects can still be an important factor in the *R*-curve behavior; see Part II).

Some of the broken specimens remained intact to a degree which left much of the grain bridging debris trapped between the crack walls. An example is shown in Fig. 11. There are clear indications of loosening and dislodging of interface-adjacent grains along the crack trace. It appears from the way some of these disturbed grains are rotated about their centers that there are intense local tractions at work. In extreme cases the intensity of these tractions is sufficient to detach the grain completely, and with some energy to spare: in some of the in situ video recording sequences individual grains occasionally disappeared along the crack trace in a single frame interval (e.g., upper left of trace in Fig. 9). Such "pop-out" events invariably occurred as the applied loading was being increased, so the tractions cannot be attributed to spurious closure forces.

For more detailed investigation of the crack-interface events, specimens of the kind shown in Fig. 11 were examined by scanning electron microscopy. Figures 12 to 14 are appropriate micrographs. Figure 12 shows clear examples of the physical contact restraints that can persist at an otherwise widely opened crack interface. Figure 13 presents a slightly more complex picture. Here the grains in the centers of the fields of view have developed secondary microfractures in the base region of attachment to one of the crack walls. There is a strong element of transgranular failure associated with this microfracture process, particularly evident in Fig. 13(A). Lastly, Fig. 14 illustrates a case in which a bridging grain has broken away from both walls and is presumably on the verge of detachment from the interface. Indeed, some minor fragments of material have already been thrown off as fracture debris, notably at lower left of the micrograph.

As with the cantilever beam specimens, evidence was sought that might reveal the presence of an extended frontal microcracking zone about the tips of arrested primary cracks in the strength specimens. Again, no such evidence was found in the SEM observations.

IV. Discussion

We have looked closely, at the microstructural level, into the processes of crack restraint in a coarse-grained alumina. This material, although ostensibly a simple, nontransforming ceramic, shows strong *R*-curve characteristics. Our observations provide clear evidence for grain-localized bridges at the newly formed crack interface behind the tip. These observations tie in with the sawcutting experiments of Knehans and Steinbrech (Section I),


5 μm

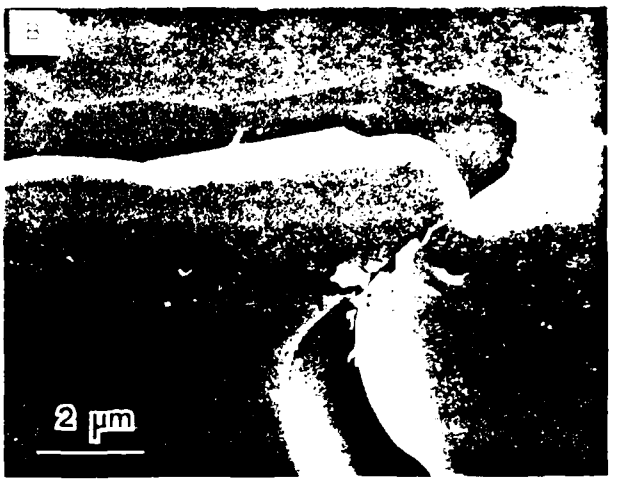
2 μm

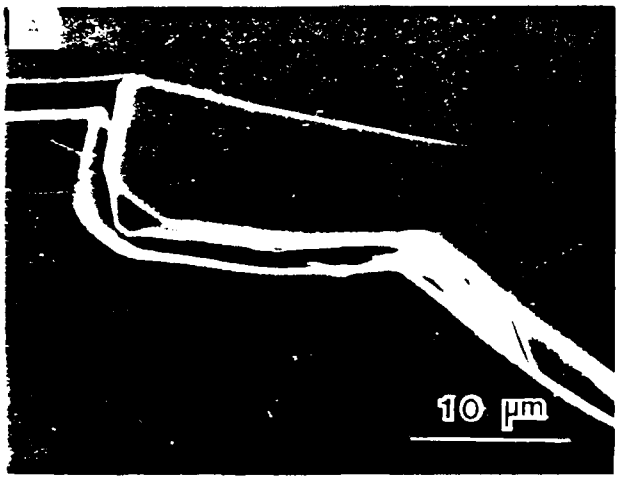
10 μm

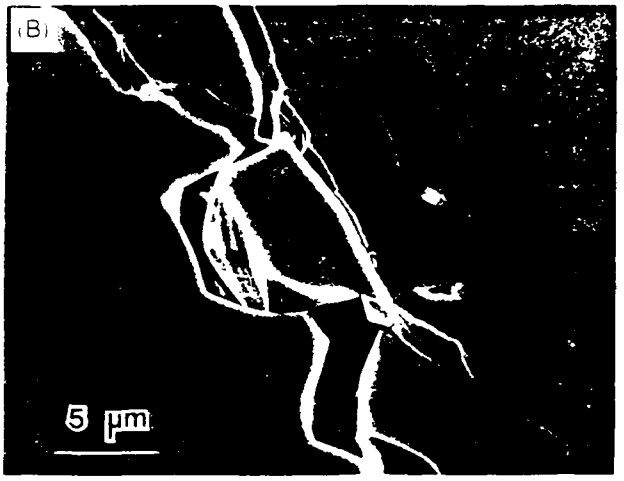
5 μm


5 μm

therefore plenty of evidence to suggest that this is a general phenomenon. As far as the present study goes, our focus on alumina does not allow us to extend this generalization to other ceramics. However, some preliminary observations on other ceramic systems in these laboratories, e.g., glass-ceramics, along with the implied universality in the *R*-curve phenomenology from the earlier, broader-based indentation-strength study[20,21] (see Section I), indicate that the interface-bridging mode may be far more widespread than hitherto suspected.

Although there appears to be little doubt about the *location* of the toughening agents in our material, the *nature* of the actual separation process remains somewhat obscure. We have presented compelling evidence for the continual development of secondary fractures, accompanied by frictional tractions, around bridging grains, confirming in large part a mechanism foreshadowed by Knehans and Steinbrech and co-workers.[14,15] However, what we have *not* been able to determine is the specific form of the discrete force-separation function that defines the micromechanics of the bridge rupture event. About all that we might say about this function is that it probably has a pronounced tail, bearing in mind the persistent activity at the bridging sites in Figs. 4 to 6 (in some cases long after one or the other of the overlapping crack segments appears to have linked up with the primary fracture surface).

The present study, in addition to identifying a most likely source of toughening in nontransforming ceramics, calls into question the validity of practically all alternative models. Recall our earlier assertion (Section I) that the evidence cited in favor of these alternative models in the literature is almost invariably circumstantial, based at best on post-mortem fractography. The popular notion of a profuse frontal microcracking zone is a prime case in point. We are unaware of any direct observation of such a zone about a growing crack in any nontransforming ceramic material (although there are some recent indications that microcracking may have a role to play in *transforming, multiphase* ceramics[28]). Our own observations gave no indication of dispersed microcracking (other than the bridging grain secondary fractures immediately adjacent to the crack walls). Yet according to the frontal-zone models[5] we would expect events in the alumina to be observable as far distant as several millimeters from the crack interface (Appendix). Moreover, one would expect to find these events manifested cumulatively as a general uprising of material adjacent to the crack trace on the free surface of the fracture specimens, since it is via a predicted dilatancy that the microcracking makes its predominant contribution to the toughening.[5] Striking examples of this kind of uprising have in fact been reported in studies on zirconia,[29,30] where the dissipation-zone description is beyond dispute. Again, the ceramics profilometry examinations revealed nothing (at least within the resolution limit of the profilometer) to support the dilatancy argument in the alumina studied here.

Reference was made in Section I to another possible model, based on crack-tip/internal-stress interactions, for explaining the *R*-curve behavior. At first sight this model does appear to be able to account for most important features of the *R* curve, especially the long range in crack sizes (relative to the grain structure) over which the toughness rises; it is argued that the microscale cracks are most likely to experience the full effect of local tensile forces but that, as extension proceeds, the cracks should gradually average out over alternative tensile and compressive grain elements.[7] However, if this were to be the whole story, the toughness of our polycrystalline alumina should saturate out at the grain boundary energy, so that, since the grain boundary is weaker than the matrix single crystal (for otherwise the fracture would be transgranular), the saturated toughness could never exceed that of sapphire. This is inconsistent with the previous indentation-strength study, where the strength-load[20] (or equivalently, toughness-load[21]) curves for polycrystalline alumina and single-crystal sapphire cross each other. Moreover, the internal stress model cannot explain the observation of *R*-curve behavior in specimens with large starter notches; the stress-averaging effect is necessarily already complete in such large crack configurations. Of course, the possibility remains that these same internal stresses could play a secondary role, by acting in concert with some other toughening mechanism, again, the absence of any abrupt increases in the crack resistance curve (i.e., on the scale of the microstructure itself) excludes certain mechanisms, e.g., deflection, pinning and bowing, as potential partners. Whether internal stresses have anything to do with the bridging mechanism advocated here, e.g., by establishing suitable conditions for creating the ligamentary elements in the first place, is a possibility that might well be explored.

In summary, our observations provide strong, direct evidence for grain-localized bridging elements as a principal source of *R*-curve behavior in nontransforming ceramics. The actual physical separation process involves secondary cracking and frictional interlocking, but the detailed micromechanics remain obscure. We have nevertheless managed to obtain some feeling for the critical dimensions involved in this process for the alumina used here. In particular, we gauge the mean bridge spacing, as reflected by the scale of discontinuous crack growth, to be ≈ 2 to 3 grain diameters, and the interfacial traction-zone length behind the crack tip to be $\gtrsim 100$ grain diameters. These dimensions will serve as a basis for our fracture mechanics modeling in Part II.

APPENDIX

Evans and Faber[5] provide a formulation of the frontal microcrack zone model from which we can estimate the spatial extent of any microcracking. Assuming that the primary-crack microcrack interaction arises principally from an averaged dilatancy within the frontal zone, yet (to a first approximation) without perturbing the stress field outside the zone, these authors take the zone width (measured perpendicular to the crack plane) as

$$h = [3^{1/2}(1 + \nu^2)^2/12\pi](K^*/\sigma_c)^2$$

where ν is Poisson's ratio, K^* is the stress intensity factor associated with the applied field, and σ_c is the critical local stress for microcrack initiation. Inserting $\nu = 0.22$, $K^* = 6.5$ MPa·m$^{1/2}$ (saturation toughness, see Part II), and $\sigma_c = 20$ MPa (estimate from Evans and Faber), we obtain $h \approx 5$ mm for our alumina.

Acknowledgments: The authors gratefully acknowledge stimulating discussions with R. F. Cook, E. R. Fuller, F. F. Lange, D. B. Marshall, R. Steinbrech and M. V. Swain during the course of this work. T. Vorburger performed the profilometer traces.

References

[1] Y.-W. Mai and B. R. Lawn, "Crack Stability and Toughness Characteristics in Brittle Materials," *Ann. Rev. Mater. Sci.*, **16**, 415–39 (1986).

[2] D. Broek, Chs. 5 and 8 in Elementary Fracture Mechanics. Martinus-Nijhoff, Boston, 1982.

[3] R. C. Garvie, R. H. Hannink, and R. T. Pascoe, "Ceramic Steel," *Nature (London)*, **258** [5537] 703–704 (1975).

[4] Advances in Ceramics, Vol. 3, Science and Technology of Zirconia. Edited by A. H. Heuer and L. W. Hobbs. American Ceramic Society, Columbus, OH, 1981.

[5] R. A. McMeeking and A. G. Evans, "Mechanics of Transformation Toughening in Brittle Materials," *J. Am. Ceram. Soc.*, **65** [2] 242–46 (1982).

[6] R. G. Hoagland and J. D. Embury, "A Treatment of Inelastic Deformation Around a Crack Tip Due to Microcracking," *J. Am. Ceram. Soc.*, **63** [7–8] 404–10 (1980).

[7] A. G. Evans and K. T. Faber, "Crack Growth Resistance of Microcracking Brittle Materials," *J. Am. Ceram. Soc.*, **67** [4] 255–60 (1984).

[8] R. W. Rice, R. C. Pohanka, and W. J. McDonough, "Effect of Stresses from Thermal Expansion Anisotropy, Phase Transformations, and Second Phases on the Strength of Ceramics," *J. Am. Ceram. Soc.*, **63** [11–12] 703–10 (1980).

[9] F. F. Lange, "The Interaction of a Crack Front with a Second-Phase Dispersion," *Philos. Mag.*, **22**, 983–92 (1970).

[10] K. T. Faber and A. G. Evans, "Crack Deflection Processes—I. Theory," *Acta Metall.*, **31** [4] 565–76; 577–84 (1983).

[11] R. Knehans and R. Steinbrech, "Memory Effect of Crack Resistance During Slow Crack Growth in Notched Al_2O_3 Specimens," *J. Mater. Sci. Lett.*, **1** [8] 327–29 (1982).

[12] A. G. Evans, A. H. Heuer, and D. L. Porter, pp. 529–56 in Fracture 1977, Vol. 1. Edited by D. M. R. Taplin. University of Waterloo Press, Ontario, Canada, 1977.

[13] H. Hubner and W. Jillek, "Subcritical Crack Extension and Crack Resistance in Polycrystalline Alumina," *J. Mater. Sci.*, **12** [11] 117–25 (1977).

[14] R. Knehans and R. Steinbrech, "Effect of Grain Size on the Crack Resistance Curves of Al_2O_3 Bend Specimens," *Sci. Ceram.*, **12**, 613–20 (1983).

[15] F. Deuerler, R. Knehans, and R. Steinbrech, "Testing Methods and Crack Resistance Behavior of Al_2O_3," to be published in *Sci. Ceram.*, Vol. 13.

[16] A. Hillerborg, M. Madeer, and P. E. Peterson, "Analysis of Crack Formation and Crack Growth in Concrete by Means of Fracture Mechanics and Finite Elements," *Cem. Concr. Res.*, **6** [6] 773–82 (1976).

[17] M. Wecharatana and S. P. Shah, "Prediction of Nonlinear Fracture Process Zone in Concrete," *J. Eng. Fract. Mech.*, **109** [5] 1231–46 (1983).

[18] P. L. Swanson, "Subcritical Fracture Propagation in Rocks: An Examination Using the Methods of Fracture Mechanics and Non-Destructive Testing," Ph.D.

Thesis, University of Colorado, Boulder, CO, 1984.
[22]P. L. Swanson, pp. 299–317 in Fracture Mechanics of Ceramics, Vol. 8. Edited by R. C. Bradt, A. G. Evans, D. P. H. Hasselman, and F. F. Lange. Plenum, New York, 1986.
[23]R. F. Cook, B. R. Lawn, and C. J. Fairbanks, "Microstructure-Strength Properties in Ceramics. I. Effect of Crack Size on Toughness," *J. Am. Ceram. Soc.*, **68** [11] 604–15 (1985).
[24]R. F. Cook, B. R. Lawn, and C. J. Fairbanks, "Microstructure-Strength Properties in Ceramics. II. Fatigue Relations," *J. Am. Ceram. Soc.*, **68** [11] 616–23 (1985).
[25]C. J. Fairbanks, B. R. Lawn, R. F. Cook, and Y.-W. Mai, pp. 23–37 in Fracture Mechanics of Ceramics, Vol. 8. Edited by R. C. Bradt, A. G. Evans, D. P. H. Hasselman, and F. F. Lange. Plenum, New York, 1986.
[26]R. F. Cook, C. J. Fairbanks, B. R. Lawn, and Y.-W. Mai, to be published in *J. Mater. Res.*
[27]D. B. Marshall, "An Improved Biaxial Flexure Test for Ceramics," *Am. Ceram. Soc. Bull.*, **59** [5] 551–53 (1980).
[28]P. L. Swanson, "Tensile-Fracture Resistance Mechanisms in Brittle Polycrystals: An Ultrasonics and In-Situ Microscopy Investigation," unpublished work.
[29]D. B. Marshall, B. R. Lawn, and P. Chantikul, "Residual Stress Effects in Sharp Contact Cracking. II. Strength Degradation," *J. Mater. Sci.*, **14** [9] 2225–35 (1979).
[30]R. G. Hoagland, A. R. Rosenfeld, and G. T. Hahn, "Mechanisms of Fast Fracture and Arrest in Steels," *Metall. Trans.*, **3** [1] 123–35 (1972).
[31]M. Rühle, N. Claussen, and A. H. Heuer, "Transformation and Microcrack Toughening as Complementary Processes in ZrO_2-Toughened Al_2O_3," *J. Am. Ceram. Soc.*, **69** [3] 195–97 (1986).
[32]M. V. Swain and R. H. J. Hannink, pp. 225–39 in Advances in Ceramics, Vol. 12, Science and Technology of Zirconia II. Edited by N. Claussen, M. Rühle, and A. H. Heuer. American Ceramic Society, Columbus, OH, 1985.
[33]D. B. Marshall, "Strength Characteristics of Transformation-Toughened Zirconia," *J. Am. Ceram. Soc.*, **69** [3] 173–80 (1986).

Reprinted from the Journal of the American Ceramic Society, Vol. 70, No. 4, April 1987
Copyright 1987 by The American Ceramic Society

Crack-Interface Grain Bridging as a Fracture Resistance Mechanism in Ceramics: II, Theoretical Fracture Mechanics Model

YIU-WING MAI† and BRIAN R. LAWN*

Ceramics Division, National Bureau of Standards, Gaithersburg, Maryland 20899

A fracture mechanics model is developed for nontransforming ceramics that show an increasing toughness with crack extension (*R*-curve, or *T*-curve, behavior). The model derives from the observations in Part I, treating the increased crack resistance as the cumulative effect of grain bridging restraints operating behind the advancing tip. An element of discreteness is incorporated into the formal distribution function for the crack-plane restraining stresses, to account for the primary discontinuities in the observed crack growth. A trial force-separation function for the local bridge microrupture process is adopted, such that an expression for the microstructure-associated crack driving (or rather, crack closing) force may be obtained in analytical form. The description can be made to fit the main trends in the measured toughness curve for a coarse-grained alumina. Parametric evaluations from such fits conveniently quantify the degree and spatial extent of the toughening due to the bridging. These parameters could be useful in materials characterization and design. It is suggested that the mechanics formulation should be especially applicable to configurations with short cracks or flaws, as required in strength analysis.

Presented at the 88th Annual Meeting of the American Ceramic Society, Chicago, IL, April 30, 1986 (Basic Science Division, Paper No. 166-B-86). Received April 16, 1986; revised copy received September 2, 1986; approved October 14, 1986.

Supported by the U.S. Air Force Office of Scientific Research; support for Y.-W. M. provided by the NBS Guest Worker Program.

*Member, the American Ceramic Society.

†On leave from the Department of Mechanical Engineering, University of Sydney, N.S.W. 2006, Australia.

I. Introduction

We have presented direct experimental evidence in Part I for a mode of crack restraint by grain-localized interfacial bridging behind the advancing tip.[1] The suggestion was made that this mode of restraint is probably a dominant mechanism of *R*-curve behavior in ceramics, at least in nontransforming ceramics. Consequently, there is a need to develop a suitable fracture mechanics model, to establish a sound basis for materials design.

This need constitutes the primary driving force for Part II of our study. We shall derive a formulation for the crack resistance as an increasing function of crack size, bounded in the lower limit by some intrinsic toughness (determined by bulk cleavage or grain boundary energies) and in the upper limit by the macroscopic toughness (representative of the microstructural composite). Following Part I, we shall again take coarse-grained alumina as our representative material, using the measured scaling dimensions for the interfacial bridging process as a basis for quantitative analysis of the observed *R* curve (or, as we shall come to call it, the *T* curve). In setting up our model we will be particularly mindful of the discontinuous (yet highly stable) nature of the crack growth during the loading to failure, most notably in the strength configurations.[1] Speaking of strength configurations, the present analysis supersedes that described in an earlier study using controlled flaws,[2,3] where the microstructural contribution to the fracture mechanics was introduced empirically without reference to any specific toughening mechanism.

An important feature of our modeling will be the capacity for separating out the fracture mechanics from the material characteristics. Essentially, our formalism requires us to specify a local force-separation relation for the restraining interfacial ligaments.

Our observations in Part I provide little clue as to what fundamental material quantities should appear in this relation, but they contain some indications as to the *form* (i.e., pronounced tail) and *spatial extent* (i.e., as determined by the critical bridging dimensions referred to above) of the functional dependence. It is thus inevitable that our treatment, while structured on a well-confirmed physical separation model, will retain an element of empiricism. We shall make use of precedents set elsewhere in deciding on an appropriate function for our alumina. This approach will preclude us from making a priori predictions of R-curve behavior in *other* materials. Accordingly, questions as to why R-curve behavior is so variable from material to material (even for materials of the same nominal composition, differing only in the grain boundary structures),[2,3] are posed as important topic areas for future researchers. Conversely, our formulation will enable us to describe the complete crack resistance behavior for a given material without explicit knowledge of the fundamental underlying separation relations.

Once again, let us foreshadow one of the ultimate goals of our study, to account for the anomalous strength characteristics shown by materials with strong R-curve behavior.[2,3] In this paper we shall confine ourselves to *qualitative* explanations of some of the more distinctive features of the crack response from indentation flaws, namely, the relative insensitivity of failure stress to flaw size at low loads and the associated growth discontinuities. A detailed quantitative treatment of the problem, in which the indentation-strength data are inverted to obtain the R curve, will be given elsewhere.[4]

II. Interfacial Crack Restraint Model

In this section we develop a fracture mechanics model for a crack restrained at its newly formed interface by distributed closure forces. These closure forces are identified with unruptured bridges whose specific nature is determined by the ceramic microstructure. As such, the restraint is analogous to that considered in the fiber-reinforced ceramic composite models,[5-7] although the underlying microstructural rupture mechanisms in the monophase materials of primary interest here may be of an entirely different kind. We shall begin with a general statement of the crack resistance problem and progressively introduce factors specific to the processes described in Part I.

(1) General Statement of Crack Resistance Problem

Our analysis here is based on equilibrium fracture mechanics, i.e., on the Griffith notion that a crack is on the verge of extension when the net mechanical driving force on the system is just equal to the intrinsic resistance (toughness) of the material.[8] The equilibrium can be stable or unstable, depending on the crack-size variation of the opposing force terms. The terminology "R curve" derives from energy release rate (G) considerations, where $R = R(c)$ is the crack-size-dependent fracture surface energy of the material. Here we shall work instead with stress intensity factors (K) because of their simple linear superposability, replacing R with an analogous toughness parameter $T = T(c)$, hence our preference for the term "T curve".[9]

Our starting point is a general expression for the net stress intensity factor for an equilibrium crack:[9]

$$K = K_a + \sum K = T_0 \tag{1}$$

$K_a = K_a(c)$ is the familiar contribution from the applied loading. The terms $K_i = K_i(c)$ represent contributions from any "internal" forces that might act on the crack, such as the microstructure-associated forces that we seek to include here. T_0 is taken to be the intrinsic material toughness (i.e., the effective K_{ic} for bulk cleavage or grain boundary fracture), strictly *independent of crack size*. Of the individual K_i terms in Eq. (1) it is only K_a which is monitored directly, via the external loading system, in a conventional fracture test. Consequently, it has become common practice to regard the K_i terms implicitly as part of the toughness characteristic. This philosophy is formalized by rewriting Eq. (1) in the form[9]

$$K_a = T = T_0 - \sum K \tag{2}$$

The quantity $T = T(c)$ defines the effective toughness function, or T curve. To obtain a rising T curve, the $K_i(c)$ functional dependencies must be either positive decreasing or negative increasing.

The existence of a rising T curve introduces a stabilizing influence on the crack growth. We have alluded to such stabilization repeatedly in Part I. From Eq. (1), the condition for the equilibrium to remain stable is that $dK/dc < 0$ (recalling that $dT_0/dc = 0$). Conversely, the condition for instability is that $dK/dc > 0$ (although satisfaction of this condition does not always guarantee failure; see Section IV). In terms of Eq. (2) the corresponding stability/instability conditions are expressible as $dK_a/dc \leqslant dT/dc$. This latter forms the basis for the conventional T-curve (R-curve) construction.

(2) Microstructure-Associated Stress Intensity Factor

Now let us consider the way in which the microstructural crack restraining forces may be folded into the fracture mechanics description. Specifically, we seek to introduce the effect of restraining bridges behind the growing crack tip as an internal stress intensity factor $K_i = K_u$. We shall focus specifically on line cracks in this paper, although this should not be seen as restricting the general applicability of the approach.

The configuration on which our model is to be based is shown in Fig. 1. The interfacial bridging ligaments are represented by the array of force centers (circles) projected onto the crack plane. (This array is depicted here as regular but in reality of course there will be a degree of variability in the distribution of centers.) Here c is the distance from the mouth to the front of the crack and d is the mean separation between closure force centers. Note that at very small crack sizes, $c < d_0$, where d_0 is the distance to the *first* bridge (not *necessarily* identical with d; see Section III), the front encounters no impedance. As the front expands, bridges are activated in the region $d_0 \leq x \leq c$. These bridges remain active until, at some critical crack dimension $c^* (\gg d)$, ligamentary rupture occurs at those sites most remote from the front. Thereafter a steady-state activity zone of length $c^* - d_0$ simply translates with the growing crack.

This configuration would appear to have all the necessary ingredients to account for the most important features in the crack response observed in Part I. The enhanced stability arises from the increasing interfacial restraint as more and more bridging sites are activated by the expanding crack. The discontinuous nature of the growth follows from the discreteness in the spatial distribution of closure forces at the crack plane. Thus the initial crack may become trapped at first encounter with the bridge energy barriers. If these barriers were to be sufficiently large the entire crack front could be retarded to the extent that, at an increased level of applied stress, the next increment of advance would occur unstably to the second set of trapping sites (pop-in). With further increase in applied stress the process could repeat itself over successive barriers, the jump frequency increasing as the expanding crack encompasses more sites within its front. There is accordingly a smoothing out of the discreteness in the interfacial restraints as the crack grows larger until ultimately, at very large crack sizes, the distribution may be taken as continuous.

In principle, we should be able to write down an appropriate stress intensity factor for any given distribution of discrete restraining forces of the kind depicted in Fig. 1. Unfortunately, the formulation rapidly becomes intractable as the number of active restraining elements becomes larger. To overcome this difficulty we resort to an approximation, represented in Fig. 2, in which the summation over discrete forces $F(x)$ is replaced by an integration over continuously distributed stresses $p(x) = F(x)/d$. These stresses have zero value in the region $x < d_0$, reflecting the necessary absence of restraint prior to intersection of the first bridging sites. They have nonzero value in the region $d_0 < x < c$ up to the crack size at which ligamentary rupture occurs ($d_0 < c < c^*$), and thereafter in the region $d_0 < c - c^* < x < c$ where a steady-state configuration obtains ($c > c^*$). This approximation is tantamount to ignoring all but the first of the discontinuous jumps in the

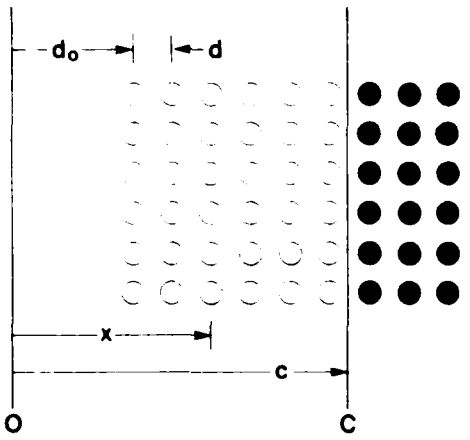

Fig. 1. Schematic of bridging model. *O* denotes origin, *C* front of crack. Circles indicate bridges, open circles denote active sites, closed circle potential sites.

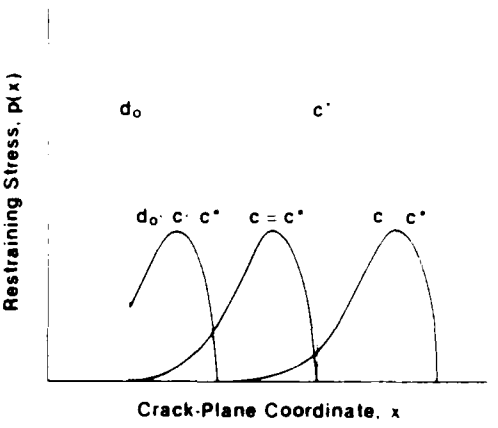

Fig. 2. Representation of bridging restraint over crack plane by continuous closure stress distribution. Distributions shown for three crack lengths c relative to d_o and c^* (see Fig. 1).

observed crack evolution. We might consider such sacrifice of part of the physical reality to be justifiable in those cases where the critical crack configuration encompasses many bridging sites, as perhaps in a typical strength test.[4]

The problem may now be formalized by writing down a microstructure-associated stress intensity factor in terms of the familiar Greens function solution for line cracks:[8,10,11]

$$K_{\mu} = 0 \qquad (d_o > c) \tag{3a}$$

$$K_{\mu} = -(2\psi/\pi)c^{1/2}\int_{d_o}^{c} p(x)\,d(x)/(c^2 - x^2)^{1/2} \qquad (d_o \le c \le c^*) \tag{3b}$$

$$K_{\mu} = -(2\psi/\pi)c^{1/2}\int_{d_o}^{c^*} p(x)\,d(x)/(c^2 - x^2)^{1/2} \qquad (c > c^*) \tag{3c}$$

where ψ is a numerical crack geometry term ($\approx \pi^{1/2}$). At this point another major difficulty becomes apparent. We have no basis, either theoretical or experimental, for specifying *a priori* what form the closure stress function $p(x)$ must take. On the other hand, we do have some feeling from Part I, albeit limited, as to the functional form $p(u)$, where u is (one half) the crack opening displacement. Moreover, it is $p(u)$ rather than $p(x)$ which should in principle (if not readily in practice) be amenable to *independent* experimental or theoretical determination. Thus, given knowledge of the crack profile, we should be able to replace x by u as the integration variable in Eq. (3), and thereby proceed one step closer to a solution.

However, even this step involves some uncertainty, since the crack profile itself is bound to be strongly influenced by the distribution of surface tractions; i.e., $u(x)$ strictly depends on $p(x)$ (as well as on the applied loading configuration), which we have just acknowledged as an unknown. A proper treatment of the fracture mechanics in such cases leads to a nonlinear integral equation,[5] for which no analytical solutions are available. With this in mind we introduce a simplification by neglecting any effect that the tractions might have on the *shape* of the profile, yet at the same time taking due account of these tractions, via the way they modify the *net* driving force K in Eq. (1), in determining the *magnitude* of the crack opening displacements. Accordingly, we choose the familiar near-field solution for a slitlike crack in equilibrium, i.e., at $K = T_{\mu}$:[10,11]

$$u(x,c) = (\sqrt{8}\psi T_{\mu}/\pi E)(c^2 - x^2)^{1/2} \tag{4}$$

where E is Young's modulus. Substitution of Eq. (4) into Eq. (3) then gives, in the approximation $d_o \to 0$ (e.g., specimens with large notches, see Section III),

$$K_{\mu} = 0 \qquad (d_o > c) \tag{5a}$$

$$K_{\mu} = -(E/T_{\mu})\int_{0}^{u(d_o,c)} p(u)\,du \qquad (d_o \le c \le c^*) \tag{5b}$$

$$K_{\mu} = -(E/T_{\mu})\int_{0}^{u^*} p(u)\,du \qquad (c > c^*) \tag{5c}$$

We point out that $u^* = u(d_o, c^*)$ is independent of c, so K_{μ} cuts off at $c \ge c^*$.

Thus by sacrificing self-consistency in our solutions, we have obtained simple working equations for evaluating the microstructure-associated stress intensity factor. We have only to specify the stress-separation function, $p(u)$.

(3) Stress-Separation Function for Interfacial Bridges

The function $p(u)$ is determined completely by the micromechanics of the ligamentary rupture process. We have indicated that we have limited information on what form this function should take. Generally, $p(u)$ must rise from zero at $u = 0$ to some maximum, and then tail off to zero again at the characteristic rupture separation u^*. There are instances in the literature where the rising portion of the curve is the all-dominant feature, e.g., as in brittle fiber-reinforced composites where abrupt failure of the ligaments cuts off an otherwise monotonically increasing frictional restraining force.[5,6] On the other hand, there are cases where the tail dominates, as in concretes where the separation process is much more stable. Our observations on the alumina in Part I would suggest that it is the latter examples which relate more closely to the polycrystalline materials of interest here. Moreover, specific modeling of *one* of the potential separation factors alluded to in Part I, frictional pullout of interlocking grains, does indeed result in a monotonically (linearly) decreasing $p(u)$ function.[7]

Thus we are led to look for a trial stress separation function which is tail-dominated. The function we choose is

$$p(u) = p^*(1 - u/u^*)^m \qquad (0 \le u \le u^*) \tag{6}$$

where p^* and u^* are limiting values of the stress and separation, respectively, and m is an exponent. This equation is illustrated by the solid curves in Fig. 3 for three values of m. $m = 0$ is the simplistic case of a uniformly distributed stress over the bridging activity zone; $m = 1$ corresponds to the frictional pullout mechanism just mentioned;[7] $m = 2$ is the value adopted empirically for fiber concretes.[11] As we shall see, m reflects most strongly in the way that the ultimate T curve cuts off in the large crack size limit.

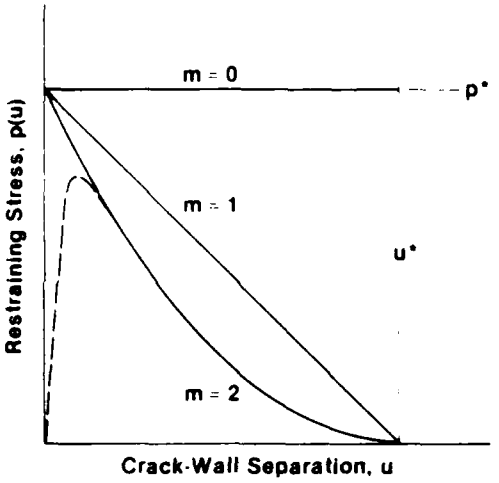

Fig. 3. Trial stress-separation function $p(u)$ for three values of exponent m in Eq. (6). Broken curve is more "realistic" function

Note that the representation is extreme in the sense that it *totally* ignores the rising portion of $p(u)$ (cf. the broken curve in Fig. 3).

Equation (6) may now be substituted into Eq. (5) and the integration carried out to give

$$K_\mu = 0 \qquad (d_0 > c) \tag{7a}$$

$$K_\mu = -(T_s - T_0)\{1 - [1 - \{(c - d_0)/(c^* - d_0)\}^{1/2}]^{m+1}\} \qquad (d_0 \le c \le c^*) \tag{7b}$$

$$K_\mu = -(T_s - T_0) \qquad (c > c^*) \tag{7c}$$

where we have made use of Eq. (4) to eliminate $u^* = u(d_0, c^*)$ in favor of c^*, i.e.

$$c^* = d_0 + (\pi E u^*/2\sqrt{2}\,\psi T_0)^2 \tag{8}$$

and where we have defined

$$T_s = T_0 + Ep^*u^*/(m + 1)T_0 \tag{9}$$

to eliminate p^*.

III. Crack Resistance Curve

We are now in a position to generate the effective toughness function from Eq. (2), i.e.

$$T(c) = T_0 - K_\mu(c) \tag{10}$$

once the parameters T_0, T_s, c^*, d_0, and m are known for any given material. Here we shall focus on the derivation of these parameters for coarse-grained alumina, leaving consideration of the crack stability (including the grain-scale discontinuities in growth referred to in Part I) to the Discussion (Section IV).

Usually, crack resistance data are obtained from test configurations which employ a starter notch, as introduced, for example, by sawcutting. The use of such a notch, in addition to providing a favorable geometry for running the crack, conveniently establishes the origin of extension at the base of the T curve. We now need to transform our coordinates, as defined in Fig. 4, we have $c = c_0 + \Delta c$, $d = c_0 + d_0$, where c_0 is the notch length. Combining Eqs. (7) and (10) then gives

$$T(\Delta c) = T_0 \qquad (d_0 > \Delta c) \tag{11a}$$

$$T(\Delta c) = T_s - (T_s - T_0)\{1 - [(\Delta c - d_0)/(\Delta c^* - d_0)]^{1/2}\}^{m+1} \qquad (d_0 < \Delta c < \Delta c^*) \tag{11b}$$

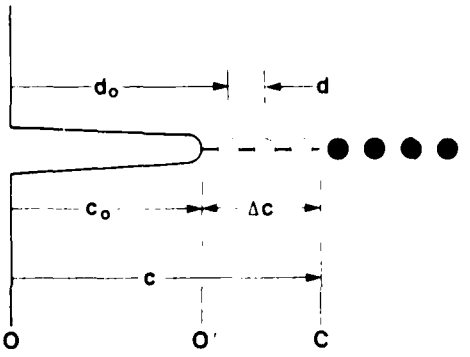

Fig. 4. Coordinates for crack system with starter notch. Effect of notch is to remove all "memory" of bridging restraints over OO', equivalent to redefining the crack origin at O'. Circles indicate bridging sites as in Fig. 1.

$$T(\Delta c) = T_s \qquad (\Delta c > \Delta c^*) \tag{11c}$$

Thus within the limits of the approximations used here (most notably the "small-scale zone" approximation used to derive Eq. (5)), we obtain a T curve which is geometry insensitive, i.e., independent of c_0. Note also that the steady-state bridging zone length from Eq. (8)

$$\Delta c^* = d + (\pi E u^*/2\sqrt{2}\,\psi T_0)^2 \tag{12}$$

is likewise geometry insensitive. We shall have more to say about this in Section IV. At this stage the rationale for our parameter definitions becomes apparent: T_0 and T_s define the lower and upper bounds, and Δc^* the spatial extent, of the T curve.

To illustrate the applicability of the formulation we examine the degree of fit of Eq. (11) to some experimental data, provided to us by M. V. Swain on a coarse-grained alumina. The material tested by Swain was of closely similar microstructure to that of the alumina used by us in Part I, i.e., reasonably large grain size (16 μm; cf. 20 μm in Part I) and nominally pure composition. He used rectangular double cantilever beam (DCB) specimens, dimensions 50 by 8 by 5 mm, notch length 11 mm, to obtain his crack data. These particular data were chosen over others in the literature because of the special precautions taken to minimize specimen end effects (see Section IV). Swain's results are plotted as the data points in Fig. 5. The theoretical fits, shown as the solid curves for fixed exponents $m = 0$, 1, and 2, were computed for trial values of $d = 50$ μm ($\approx$3 grain diameters) and $\Delta c^* = 10$ mm ($\approx$600 grain diameters) in accordance with the estimates from Part I, with T_0 and T_s as regression adjustables.

A word of caution is in order here. Any "goodness of fit" that we might consider evident in Fig. 5 may properly be taken as lending credence to our model. However, it should not be seen as constituting *proof* of our model. In essence, our equations contain five parameters whose values are, to a greater or lesser extent, unknown a priori. Thus, for instance, the accuracy of the fit is not sensitive to the trial value of d, but it *is* sensitive to Δc^* (reflecting the fact that the DCB data are weighted toward the region $\Delta c \gg d$). Such sensitivity to the choice of any *one* parameter inevitably contributes to the uncertainty in the *other* parameters. Consequently, despite all outward appearances in Fig. 5, we would be reluctant to assert that $m = 0$ is the "true" value of the toughness exponent.

Notwithstanding these uncertainties in the parameter determinations, we may usefully estimate the force-separation parameters p^* and u^* in Eq. (6). Thus, substituting $E = 400$ GPa, $\psi = \pi$ (ideal line cracks), along with the best fit values of T_s into Eq. (12) gives $u^* = 1$ μm (independent of m). This is of the order of the crack opening displacements evident in the micrographs in Part I. Further substitution together with the regressed T_s values into Eq. (9) gives $p^* = 25$ MPa ($m = 0$), 40 MPa

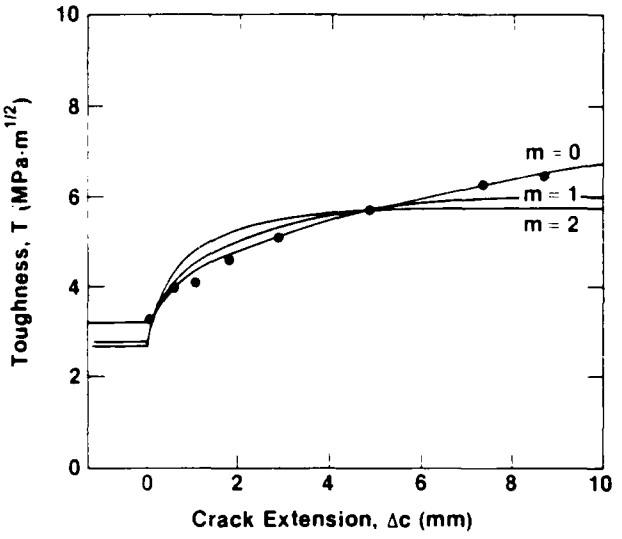

Fig. 5. Fit of Eq. (11) to double cantilever beam (DCB) toughness data on coarse-grained alumina. Fits are for $d = 50\ \mu m$, $\Delta c^* = 10$ mm, and $m = 0$, 1, and 2, with T_0 and T_∞ as adjustables. (Data courtesy M. V. Swain.)

($m = 1$), and 55 MPa ($m = 2$). If these stress levels seem low, we may note that the composite quantity $p^*u^*/(m + 1)$, which represents the work per unit area to separate the bridges across the fracture plane (see integral in Eq. 5(c)), is of order 20 $J \cdot m^{-2}$, i.e., comparable with typical fracture surface energies.

Finally in this section, let us note that we have yet to address the issue of crack *instabilities* in the T-curve characteristic. Recall that our analysis smoothes out all but the very first bridge discontinuity, i.e., at $c = d_0$, the data in Fig. 5 are insufficiently detailed in this region to allow any quantitative resolution of this question. We need to go to short-crack configurations. An account of the T-curve construction for such configurations is deferred to Section IV.

IV. Discussion

We have derived a T-curve (R-curve) model based on bridging tractions at the crack interface behind the advancing tip. The model contains several adjustable parameters, but parameters to which we may nonetheless attach physical meaning. Thus the spatial parameters c^* (Δc^*) and d_0, respectively, define the *range* of the T curve and the *characteristic separation* between bridging elements. The toughness parameters T_0 and T_∞ respectively define the *base crack resistance* in the absence of microstructural restraints (lower limit to T curve) and the *macroscopic crack resistance* (upper limit). Then we have the parameters m, p^*, and u^*, which determine the empirical force-separation "law" for the bridging process. These parameters, once evaluated for a given material, could be useful in structural design.

It is instructive to consider how the present treatment of the microstructural contribution to crack resistance characteristics differs from that proposed in an earlier study of indentation-strength systems.[17] In that study the microstructure-associated stress intensity factor K_r (cf. $K_{\mu\infty}$ used in this work) was introduced in terms of an empirical grain-localized driving force at the radial crack center, in direct analogy to the (well-documented) residual-contact force field.[4,5] There, K_r was defined as a *positive* term *decreasing* with respect to crack size, with T_0 as the reference toughness level (i.e., the level at which $K_r = 0$). Here, K_μ is defined as a *negative* (closure) term *increasing* with respect to crack size, with T_0 to the reference toughness level ($K_\mu = 0$). Conventional fracture mechanics measurements, i.e., measurements of crack size as a function of applied load, cannot in themselves distinguish between these two alternative K descriptions. It is in this context that the direct observations in Part I may be seen as critical. Moreover, the new model has its roots in a positively identifiable toughening mechanism, so taking us one step closer to a fundamental base for a priori predictions.

However, it needs to be reemphasized that the element of empiricism has not been entirely eliminated in the present treatment. There is the issue of the force-separation relation $p(u)$, which we have represented by the tail-dominated function in Eq. (6). Ideally, we would like to be able to determine $p(u)$ from first principles, but this would require a more detailed understanding of the grain bridging micromechanisms than is available at present. Only then may we hope to specify what intrinsic material properties, other than E and T_0 (see Eq. (5)), govern the toughness behavior. At that stage we may be in a position to answer some of the more pressing questions that arise in connection with observed T-curve trends. Thus, what is the explicit dependence of toughness on grain size, and (perhaps more intriguingly) what is it about the incorporation of a glassy grain boundary phase which so dramatically washes out the T-curve effect?[2,3] What role do internal microstresses play? It is with such issues that our ultimate ability to tailor superior structural ceramics must surely rest.

There are other limitations of our analysis which warrant further comment, particularly in relation to geometric effects. In our quest for an analytical solution to the fracture mechanics equations we have resorted to a questionable approximation of the crack-wall displacement profile, Eq. (4). Quite apart from the fact that this approximation is strictly justifiable only for traction-free walls, i.e., in clear violation of the very boundary conditions that we seek to incorporate into our analysis, it requires that we should not attempt to extend the description beyond the confines of the near field. Yet the results of our experimental observations in Part I show bridging activity zones of order millimeters, which is by no means an insignificant length in comparison to typical test specimen dimensions. Thus, contrary to the predictions of Eq. (11), we should not be surprised to find a strong geometry dependence in the measured T-curve response. Such a dependence has been observed in practice, particularly in single-edge-notched beam specimens of alumina with different starter notch lengths.[18,19] There are in fact reported instances, in fiber-reinforced cements,[20] where specimen size effects can *dominate* the intrinsic component in the T-curve characteristic. This is an added concern for the design engineer, whose faith in the T-curve construction is heavily reliant on our ability to prescribe $T(c)$ as a true material property.

Notwithstanding the above reservations, let us return to the question of crack growth discontinuities raised toward the end of Section III. It was pointed out that we need to consider short cracks, i.e., cracks smaller in length than the distance to the first bridging sites, and indeed preferably smaller than the mean bridge spacing itself. This is, of course, the domain of natural flaws. The indentation method is one way of introducing cracks of this scale, with a high degree of control, and will be the subject of a detailed quantitative analysis elsewhere.[4] For the present, we simply consider such a crack, but without residual contact stresses, subjected to a uniformly applied tensile stress, σ_∞. Figure 6 is a schematic T-curve construction for this system, showing how the initial crack at $c_i < d$ evolves as the applied stress is increased to failure. The plot is in normalized logarithmic coordinates, to highlight the response at small c. This same plotting scheme allows for a convenient representation of the applied stress intensity factor, $K_\infty = \psi\sigma_\infty c^{1/2}$, as a family of parallel lines of slope $\frac{1}{2}$ at different stress levels. The sequence of events is then as follows: (i) at loading stage 1, $K_\infty = K_{\mu\infty}(\sigma_\infty)$, the crack remains stationary, (ii) at stage 2, the crack attains equilibrium at $K_\infty = T(c)$, and extends from an unstable state at $J(dK_\infty/dc) = dT/dc$ to a stable state at $J(dK_\infty/dc) < dT/dc$, (iii) on increasing the load to stage 3, the crack propagates stably through J to I_∞ up the T curve, (iv) at stage 4, a tangency condition is achieved at M, whence failure occurs. Thus our model has the capacity to account for the first crack jump discontinuity (pop-in), as well as the enhanced stability we have come to associate with this class of material.

As a corollary of the construction in Fig. 6, note that the critical loading condition at M is not affected in any way by the initial

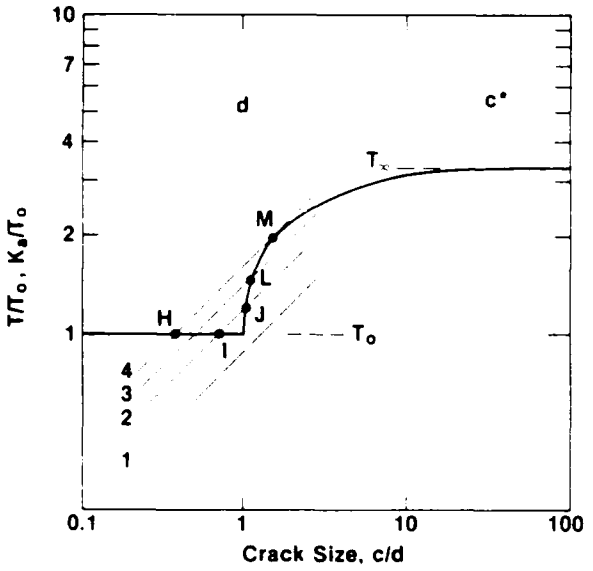

Fig. 6. T-curve construction for short crack ($c_i \leq c_o \leq c_M$). Solid curve is $T(c)$ function. Inclined dashed lines 1 → 4 represent K_a loading lines for successively increasing values of applied stress σ. Crack "pops in" along IJ at stage 2 in the stressing, then progresses through JLM along curve to failure at stage 4. Note failure stress is determined exclusively by tangency condition at M, independent of initial crack size.

crack size c_o provided this initial size falls within the range $c_H \leq c_o \leq c_M$. This explains why the strengths of specimens containing controlled flaws tend to level off at diminishing crack size (indentation load). Thus we have a region of "flaw tolerance," a desirable quality from the standpoint of engineering design.

Finally, we are led to believe that the notion of crack interface bridging may have a far greater generality in the accounting of T-curve behavior in ceramics than previously suspected. We have singled out coarse-grained alumina for special study, but the earlier indentation-strength studies on a wide range of materials suggests a certain commonality in the underlying mechanisms of toughening. At the same time, the validity of popular alternative models, particularly those founded on the hypothesis of a dispersed microcracking zone, is in serious doubt. These strong conclusions derive primarily from the direct observations described in Part I. The use of such observations as a means of identifying the responsible toughening mechanisms has been conspicuously absent in the ceramics literature. There is a clear need to develop the present treatment further, especially in regard to the bridging force-separation function. Further, the formulation should be extended to include *non*equilibrium states, where the T curve is expected to manifest itself in intriguing ways, e.g., in fatigue limits and non-unique crack velocity ($v(K_a)$) functions. Our model is just the first step to a proper understanding of the toughness behavior of materials in terms of microstructural variables, which we must ultimately control if the goal of the property-tailored ceramic is ever to be realized.

Acknowledgments: The authors thank the following for their discussions on various aspects of this work: R. F. Cook, C. J. Fairbanks, E. R. Fuller, B. J. Hockey, D. B. Marshall, and P. L. Swanson. M. V. Swain kindly provided us with the data for Fig. 5 before publication.

References

[1]P. L. Swanson, C. J. Fairbanks, B. R. Lawn, Y. W. Mai, and B. J. Hockey, "Crack-Interface Grain Bridging as a Fracture Resistance Mechanism in Ceramics: I. Experimental Study on Alumina," this issue, preceding article.
[2]R. F. Cook, B. R. Lawn, and C. J. Fairbanks, "Microstructure-Strength Properties in Ceramics: I. Effect of Crack Size on Toughness," *J. Am. Ceram. Soc.* **68** [11] 604–15 (1985).
[3]R. F. Cook, B. R. Lawn, and C. J. Fairbanks, "Microstructure-Strength Properties in Ceramics: II. Fatigue Relations," *J. Am. Ceram. Soc.* **68** [11] 616–23 (1985).
[4]R. F. Cook, C. J. Fairbanks, B. R. Lawn, and Y.-W. Mai, to be published in *J. Mater. Res.*
[5]D. B. Marshall and A. G. Evans, pp. 557–68 in Proceedings of the 5th International Conference on Composite Materials. Edited by W. C. Harrigan, J. Strife, and A. K. Dhingra. Metallurgical Society of A.I.M.E., Warrendale, PA, 1985.
[6]D. B. Marshall, B. N. Cox, and A. G. Evans, "The Mechanics of Matrix Cracking in Brittle-Matrix Fiber Composites," *Acta Metall.* **33** [11] 2013–21 (1985).
[7]D. B. Marshall and A. G. Evans, pp. 1–15 in Fracture Mechanics of Ceramics, Vol. 7. Edited by R. C. Bradt, A. G. Evans, D. P. H. Hasselman, and F. F. Lange. Plenum, New York, 1986.
[8]B. R. Lawn and T. R. Wilshaw, Ch. 3 in Fracture of Brittle Solids. Cambridge University Press, London, 1975.
[9]Y.-W. Mai and B. R. Lawn, "Crack Stability and Toughness Characteristics in Brittle Materials," *Annu. Rev. Mater. Sci.* **16**, 415–39 (1986).
[10]G. I. Barenblatt, "The Mathematical Theory of Equilibrium Cracks in Brittle Fracture," *Adv. Appl. Mech.* **7**, 55–129 (1962).
[11]H. Tada, P. C. Paris, and G. R. Irwin, Part III in The Stress Analysis of Cracks Handbook. Paris Productions, St. Louis, MO, 1985.
[12]A. G. Evans, A. H. Heuer, and D. L. Porter, pp. 529–56 in Fracture 1977, Vol. 1. Edited by D. M. R. Taplin. University of Waterloo Press, Ontario, Canada, 1977.
[13]R. Ballarini, S. P. Shah, and L. M. Keer, "Crack Growth in Cement Based Composites," *Eng. Fract. Mech.* **20** [3] 433–45 (1984).
[14]D. B. Marshall and B. R. Lawn, "Residual Stress Effects in Sharp-Contact Cracking: I. Indentation Fracture Mechanics," *J. Mater. Sci.* **14** [9] 2001–12 (1979).
[15]B. R. Lawn, A. G. Evans, and D. B. Marshall, "Elastic/Plastic Indentation Damage in Ceramics: The Median/Radial Crack System," *J. Am. Ceram. Soc.* **63** [9–10], 574–81 (1980).
[16]R. Knehans and R. Steinbrech, "Memory Effects of Crack Resistance During Slow Crack Growth in Notched Al_2O_3 Specimens," *J. Mater. Sci. Lett.* **1** [8] 327–29 (1982).
[17]F. Deuler, R. Knehans, and R. Steinbrech, "Testing Methods and Crack Resistance Behavior of Al_2O_3," to be published in *Sci. Ceram.*, Vol. 13.
[18]H. Hubner and W. Jillek, "Subcritical Crack Extension and Crack Resistance in Polycrystalline Alumina," *J. Mater. Sci.* **12** [1] 117–25 (1977).
[19]H. Wieninger, K. Kromp, and R. F. Pabst, "Crack Resistance Curves of Alumina and Zirconia at Room Temperature," *J. Mater. Sci.* **21** [2] 411–18 (1986).
[20]R. M. L. Foote, B. Cotterell, and Y. W. Mai, pp. 135–44 in Advances in Cement Matrix Composites. Edited by D. M. Roy. Materials Research Society, Pennsylvania, 1980.

Crack resistance by interfacial bridging: Its role in determining strength characteristics

Robert F. Cook
IBM, Thomas J. Watson Research Center, Yorktown Heights, New York 10598

Carolyn J. Fairbanks, Brian R. Lawn, and Yiu-Wing Mai[a)]
Ceramics Division, National Bureau of Standards, Gaithersburg, Maryland 20899

(Received 27 October 1986; accepted 3 March 1987)

An indentation-strength formulation is presented for nontransforming ceramic materials that show an increasing toughness with crack length (T curve, or R curve) due to the restraining action of interfacial bridges behind the crack tip. By assuming a stress-separation function for the bridges a microstructure-associated stress intensity factor is determined for the penny-like indentation cracks. This stress intensity factor opposes that associated with the applied loading, thereby contributing to an *apparent* toughening of the material, i.e., the measured toughness in excess of that associated with the intrinsic cohesion of the grain boundaries (intergranular fracture). The incorporation of this additional factor into conventional indentation fracture mechanics allows the strengths of specimens with Vickers flaws to be calculated as a function of indentation load. The resulting formulation is used to analyze earlier indentation-strength data on a range of alumina, glass–ceramic, and barium titanate materials. Numerical deconvolution of these data determines the appropriate T curves. A feature of the analysis is that materials with pronounced T curves have the qualities of flaw tolerance and enhanced crack stability. It is suggested that the indentation-strength methodology, in combination with the bridging model, can be a powerful tool for the development and characterization of structural ceramics, particularly with regard to grain boundary structure.

I. INTRODUCTION

Recent studies have shown that many polycrystalline, non-phase-transforming ceramics exhibit an increasing resistance to crack propagation with crack length.[1–4] At small flaw sizes, comparable to the scale of the microstructure, the toughness T is an intrinsic quantity representative of the weakest fracture path. At large flaw sizes the toughness tends to a higher, steady-state value representative of the cumulative crack/microstructure interactions in the polycrystal. The progressive transition from the low-to-high toughness limits during crack extension is described as the T curve. [The concepts of T curve and R curve are equivalent.[5] In the former the equilibrium condition is obtained by equating the net stress intensity factor K, characterizing the net applied load on the crack, to the toughness T (alternatively designated K_{IC} in some of the earlier literature) characterizing critical crack resistance forces. In the latter, the mechanical energy release rate G, derived from the work done by the applied loading during crack extension, is equated to the energy necessary to create the fracture surfaces R.]

Perhaps the most comprehensive studies of this T-curve behavior have been made using a controlled flaw technique,[1–4] in which the strengths of specimens containing indentations are measured as a function of indentation load. It was found that, for large flaws, the strengths tend to an "ideal" $-\frac{1}{3}$ power law dependence of strength on indentation load, indicative of a nonvarying toughness. At small flaw sizes, however, the strengths decrease markedly from this ideal behavior, tending instead to a load-independent plateau. Significantly, in a group of polycrystalline alumina materials it was found that the strengths at large flaw sizes were all greater than those of single-crystal sapphire, whereas the reverse tended to be true at small flaw sizes.[1] Taken with the observation that the fracture in these aluminas is intergranular, these results suggest that the grain boundaries are paths of weakness but that there is some mechanism operating that more than compensates for this intrinsic weakness as the flaw size increases. Moreover, the strength-load responses of the polycrystalline materials themselves, even those with similar grain sizes, tended to cross each other.[1] It would appear that the nature of the grain boundary, as well as the grain size, influences the fracture behavior.

Two other sets of experiments provide vital clues as to the mechanism of crack/microstructure interaction

[a)] On leave from the Department of Mechanical Engineering, University of Sydney, New South Wales 2006, Australia.

underlying the T-curve behavior. In the first set, Knehans and Steinbrech[9] propagated large cracks in alumina using the single-edge-notched beam geometry. They observed strongly rising T-curves as cracks propagated from the tip of the notch. However, when interfacial material was removed from behind the crack tip by careful sawing, the toughness did not continue up the T curve but reverted to its original level, implying that the critical mechanism must be operating in the "wake" of the crack tip. In the second set of experiments, Swanson *et al.*[8] observed crack propagation in alumina using both indented-disk and tapered-cantilever beam specimens. Active grain-localized "bridges" were observed at the primary crack interface, over a "zone length" of millimeter scale. The implication here is that interfacial bridging ligaments *behind* the tip are providing a restraining influence on crack extension. The reversion to the base of the T curve in the experiments of Knehans and Steinbrech may be interpreted in terms of the removal of these restraining ligaments.

Mai and Lawn[10] developed a fracture mechanics model for the propagation of ligamentary bridged cracks, incorporating parameters characterizing the interbridge spacing, the intrinsic intergranular toughness, and the force-extension "law" for the bridges. They applied the model to the propagation of full-scale cracks propagating under double cantilever loading and thereby demonstrated consistency with the measured T-curve response in a polycrystalline alumina.

Here we shall apply the Mai–Lawn bridging model to the mechanics of the indentation-strength test. It is appropriate to do this for two reasons. First, indentation cracks are strongly representative of the small "natural" flaws that control the strengths of ceramic materials in service.[1] Second, and most important, the indentation methodology will be seen to be ideally suited to quantitative analysis of the T-curve function. For this purpose, recourse will be made to several earlier sources of indentation-strength data, covering a broad spectrum of ceramic materials.[1,3,4,11] The consequent manner in which the indentation-strength test highlights one of the most important manifestations of T-curve behavior, namely flaw tolerance, will emerge as a uniquely appealing feature of the approach. The potential for using the attendant parametric evaluations in the T-curve analysis as a tool for investigating the role of chemical composition and processing variables as determinants of toughness properties is indicated.

II. INTERFACIAL CRACK RESTRAINT MODEL

An earlier fracture mechanics model[10] for straight-fronted cracks restrained by interfacial bridging ligaments is reproduced here in modified form, appropriate to penny-like indentation cracks.

A. Equilibrium crack propagation

A fracture system is in equilibrium when the forces driving the crack extension are equal to the forces resisting this extension. Equilibria may be stable or unstable, depending on the crack-length dependence of these forces.[4] Here we shall characterize the driving forces by stress intensity factors $K(c)$ and the fracture resistance by toughness $T(c)$, where c is the crack size. We may consider separately the stress intensity factor arising from the applied loading K_a, which is directly monitored, from that associated with any internal forces intrinsic to the microstructure K_i, such as the ligamentary bridging forces we seek to include here. We may then conveniently regard the fracture resistance of the material as the sum of an intrinsic interfacial toughness of the material T_0 and the internal K_i terms.[4] Hence our condition for equilibrium may be written

$$K_a(c) = T(c) = T_0 - \sum K_i(c), \qquad (1)$$

where we have summed over all internal contributions. We emphasize that T_0 is strictly independent of crack length. The quantity $T(c)$ is the effective toughness function, or T curve, for the material. To obtain a rising T curve, i.e., an increase in toughness with crack length, the sum over the $K_i(c)$ terms must be either positive decreasing or negative increasing. In terms of Eq. (1) the condition for stability is that $dK_a/dc < dT/dc$ and for instability $dK_a/dc > dT/dc$.[4] We see then that a rising T curve, where $dT/dc > 0$, will lead to increased stabilization of the crack system.

B. Microstructure-associated stress intensity factor

We seek now to incorporate the effect of restraining ligaments behind the growing crack tip into a microstructure-associated stress intensity factor, $K_i = \Sigma K_i$. In the context of indentation flaws we shall develop the analysis for cracks of half-penny geometry.

A schematic model of the proposed system is shown in Fig. 1. The interfacial bridging ligaments are represented as an array of force centers, $F(r)$, projected onto the crack plane. Here c is the radius of the crack front and d is the characteristic separation of the centers. At very small cracks sizes, $c < d$, the front encounters no impedance. As the front expands, bridges are activated in the region $d \le r \le c$. These bridges remain active until, at some critical crack size $c^* (\gg d)$, ligamentary rupture occurs at those sites most distant behind the front. Thereafter a steady-state annular zone of width $c^* - d$ simply expands outward with the growing crack.

The qualitative features of the crack response observed by Swanson *et al.*[8] would appear to be well described by the above configuration. Enhanced crack sta-

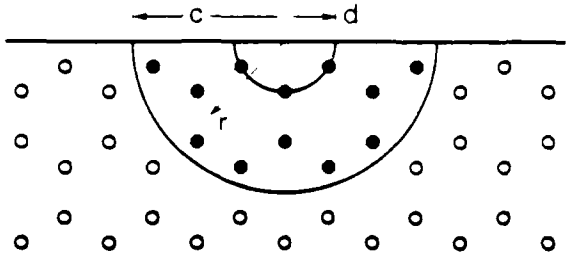

FIG. 1. Schematic diagram of a half-penny, surface crack propagating through a material with bridging ligaments impeding the crack motion. Here d is the mean ligament spacing, c is the crack radius, and r is the radial coordinate from the penny origin; ● denotes the active ligament sits and ○ denotes potential ligament sites.

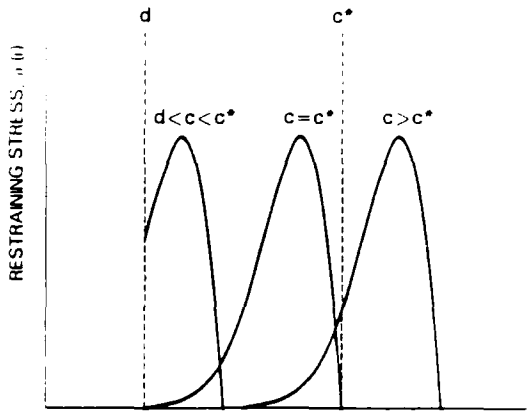

FIG. 2. Stress distribution applied by the restraining ligaments over the crack plane as a function of radial distance from the center of the crack. Note that the stress is zero for $r < d$ and reaches a steady-state distribution for $c > c^*$.

bility arises from the increasing interfacial restraint as more and more bridging sites are activated by the expanding crack front (the number of active bridges will increase approximately quadratically with the crack radius). The discontinuous nature of the crack growth follows from the discreteness in the spatial distribution of the closure forces in the crack plane. Thus we imagine the crack to become trapped at first encounter with the barriers. If these barriers were to be sufficiently large the crack front could be "trapped" such that, at an increased level of applied stress, the next increment of advance would occur unstably to the second set of trapping sites. Further increases in applied stress would lead to repetitions of this trapping process over successive barriers, the jump frequency increasing as the expanding crack front encompasses more sites. There must accordingly be a smoothing out of the discreteness in the distribution of interfacial restraints as the crack grows until, at very large crack sizes, the distribution may be taken as continuous. With regard to the steady-state zone width $(c^* - d)$ referred to above, our own observations and those of Swanson *et al.*[8,12] indicate that, for a given material, there is a characteristic distance behind the crack tip that contains apparently intact bridges.

In principle, we should be able to write down an appropriate stress intensity factor for any given distribution of discrete restraining forces of the kind depicted in Fig. 1. However, an exact summation becomes intractable as the number of active restraining elements becomes large. To overcome this difficulty we approximate the summation over the discrete force elements $F(r)$ by an integration over continuously distributed stresses $\sigma(r) \simeq F(r)/d^2$. We plot these stresses for three crack configurations in Fig. 2. These stresses have zero value in the region $r < d$, reflecting the necessary absence of restraint prior to the intersection of the crack front with the first bridging sites. They have nonzero value in the region $d < r < c$ up to the crack size at which ligamentary rupture occurs $(d \leq c \leq c^*)$ and thereafter in the region $d + c - c^* < r < c$, where a steady-state configuration is obtained $(c > c^*)$. This approximation is tantamount to ignoring all but the first of the discontinuous jumps in the observed crack evolution. We might consider such a sacrifice of part of the physical reality to be justifiable in those cases where the critical crack configuration encompasses many bridging sites, as perhaps in a typical strength test.

The problem may now be formalized by writing down a microstructure-associated stress intensity factor in terms of the familiar Green's function solution for penny-like cracks[13]:

$$K_u = 0 \quad (c < d), \tag{2a}$$

$$K_u = -\left(\frac{\psi}{c^{1/2}}\right)\int_d^c \sigma(r)\, r\, \frac{dr}{(c^2 - r^2)^{1/2}} \quad (d \leq c \leq c^*), \tag{2b}$$

$$K_u = -\left(\frac{\psi}{c^{1/2}}\right)\int_{d+c-c^*}^{c} \sigma(r)\, r\, \frac{dr}{(c^2 - r^2)^{1/2}} \quad (c > c^*), \tag{2c}$$

where ψ is numerical crack geometry term. At this point another major difficulty becomes apparent. We have no basis, either theoretical or experimental, for specifying *a priori* what form the closure stress function $\sigma(r)$ must take. On the other hand, we do have some feeling from the observations of Swanson *et al.*, albeit limited, as to the functional form $\sigma(u)$, where u is the crack opening displacement. Further, it is $\sigma(u)$ rather than $\sigma(r)$ that

is the more fundamental bridging quantity and that is more amenable to independent specification. Thus, given a knowledge of the crack profile, we should be able to replace r by u as the integration variable in Eq. (2) and thereby proceed one step closer to a solution.

However, even this step involves some uncertainty, as the crack profile itself is bound to be strongly influenced by the distribution of surface tractions, i.e., $u(r)$ strictly depends on $\sigma(r)$ (as well as on the applied loading configuration), which we have just acknowledged as an unknown. A rigorous treatment of this problem involves the solution of two coupled nonlinear integral equations, for which no analytical solutions are available.[14] We thus introduce a simplification by neglecting any effect the tractions might have on the *shape* of the crack profile, while taking account of these tractions through their influence on the net driving force $K = K_a - K_\mu$ from Eq. (1), in determining the *magnitude* of the crack opening displacements. Accordingly, we choose Sneddon's solution[15] for the near-field displacements of an equilibrium crack, i.e., $K = T_0$,

$$u(r,c) = (\psi T_0/Ec^{1/2})(c^2 - r^2)^{1/2}, \tag{3}$$

where E is the Young's modulus. Substitution of Eq. (3) into Eq. (2) then gives

$$K_a = 0 \quad (c < d), \tag{4a}$$

$$K_a = -\left(\frac{E}{T_0}\right)\int_0^{u(d,c)} \sigma(u)du \quad (d \le c \le c^*), \tag{4b}$$

$$K_a = -\left(\frac{E}{T_0}\right)\int_0^{u^*} \sigma(u)du \quad (c > c^*). \tag{4c}$$

We note that $u^* = u(d,c^*)$ is independent of c so K_μ cuts off at $c > c^*$.

Let us note here that our choice of the Sneddon profile, Eq. (3) leads us to an especially simple solution for K_a in Eq. (4). In particular, we note that this term is conveniently expressible as an integral of the surface closure stress as a function of the crack opening displacement, i.e., a work of separation term. This simple solution obtains *only* with the Sneddon profile. It might be argued that a Dugdale-type profile[16] is more appropriate, but it can be shown that the fracture mechanics are not too sensitive to the actual profile chosen.[17] Our main objective here is to emphasize the physical variables involved. Thus by sacrificing self-consistency in our solutions, we have obtained simple working equations for evaluating the microstructure-associated stress intensity factor. We have only to specify the stress-separation function $\sigma(u)$.

C. Stress-separation function for interfacial bridges

The function $\sigma(u)$ is determined completely by the micromechanics of the ligamentary rupture process. We have indicated that we have limited information on what form this function should take. Generally, $\sigma(u)$ must rise from zero at $u = 0$ to some maximum and then decrease to zero again at some characteristic rupture separation u^*. The observations of crack propagation in alumina by Swanson *et al.* suggest that it is the decreasing part of this stress-separation response that is the most dominant in the polycrystalline ceramics of interest here.[3] The stable crack propagation observed by those authors has much in common with the interface separation processes in concrete materials that are often described by tail-dominated stress-separation functions.

The stress-separation function chosen is[10]

$$\sigma(u) = \sigma^*(1 - u/u^*)^m \quad (0 \le u \le u^*), \tag{5}$$

where σ^* and u^* are limiting values of the stress and separation, respectively, and m is an exponent. We consider three values of m: $m = 0$ is the simplest case of a uniformly distributed stress acting over the annular activity zone; $m = 1$ corresponds to simple, constant-friction pullout of the interlocking ligamentary grains. $m = 2$ is the value adopted by the concrete community (equivalent to a decreasing frictional resistance with increasing pullout). As we shall see, the choice of m will not be too critical in our ability to describe observed strength data. Note that the representation of the stress-separation function by Eq. (5) is an infinite modulus approximation in that it totally neglects the rising part of the $\sigma(u)$ response.

Equation (5) may now be substituted into Eq. (4) to yield, after integration,

$$K_\mu = 0 \quad (c < d), \tag{6a}$$

$$K_\mu = -(T_\infty - T_0)(1 - \{1 - [c^*(c^2 - d^2)^{1/2} - c(c^{*2} - d^2)^{1/2}]^{m+1}\}^{m+1}) \quad (d \le c \le c^*), \tag{6b}$$

$$K_\mu = -(T_\infty - T_0) \quad (c > c^*), \tag{6c}$$

where we have eliminated the stress-separation parameters σ^* and u^* in favor of those characterizing steady-state crack propagation, c^* and T_∞:

$$c^* = 2(Eu^*/\psi T_0)^2\{1 + [1 + 4(\psi T_0 d^{1/2}/Eu^*)^4]^{1/2}\} \tag{7}$$

and

$$T_\infty = T_0 + E\sigma^*u^*/(m-1)T_0. \tag{8}$$

These latter parameters are more easily incorporated into the strength analysis to follow.

A useful quantity is the work necessary to rupture an individual ligament. This work is a composite measure of the maximum sustainable stress and maximum range of the stress-extension function of Eq. (5) and is given by the area under the stress-separation curve $\sigma(u)$. We may express this area as

$$\Gamma = \int_0^{u^*} \sigma(u)du = \frac{\sigma^*u^*}{(m+1)} \tag{9a}$$

It is useful to compare this quantity with the intrinsic interfacial energy[9]

$$\Gamma_0 = T_0^2/2E. \tag{9b}$$

The Γ terms in Eq. (9) are related, through Eq. (8), by the ratio

$$\Gamma_s/\Gamma_0 = 2(T_\infty - T_0)/T_0, \tag{10}$$

which may conveniently be regarded as a toughening index.

D. Strength-indentation load relations

We are now in the position to consider the mechanics of a test specimen containing an indentation crack produced at load P and subsequently subjected to an applied stress σ_a. To obtain the "inert strength" σ_m, we need to determine the equilibrium instability configuration at which the crack grows without limit.

In indentation crack systems the stress intensity factor associated with the residual contact stresses K_r augments the stress intensity factor associated with the applied loading K_a effectively giving rise to a *net* applied stress intensity factor K_a'.[18,19] Equation (1) becomes

$$K_a' = K_a + K_r = T(c)$$
$$= \psi\sigma_a c^{1/2} + \chi P/c^{3/2} = T_0 - K_\mu(c), \tag{11}$$

where χ measures the intensity of the residual field. We note that K_r is inverse in crack size and hence will further stabilize the fracture evolution.[19] The indentation load determines the initial crack size at $\sigma_a = 0$, but *because* of the stabilization in the growth we should not necessarily expect this initial size to be an important factor in the fracture mechanics. Our problem then is to combine Eqs. (6) and (11) and invoke the instability condition $dK_a'/dc \geq dT/dc$ to determine the strength as a function of indentation load.

Unfortunately, it is not possible to obtain closed form solutions to this problem. Limiting solutions *can* be obtained analytically, however, and we consider these first.

(*i*) *Small cracks (low P)*. In the region $c \ll d$ we revert to the ideal case of zero microstructural interaction, such that Eq. (6a) applies. In this region it can be readily shown that the equilibrium function $\sigma_a(c)$ obtained by rearranging Eq. (11) passes through a maximum, up to which point the crack undergoes stable growth.[19] This maximum therefore defines the instability point $d\sigma_a/dc = 0$ (equivalent to the condition $dK_a'/dc = dT/dc = 0$ here):

$$\sigma_m^0 = 3T_0^{4/3}/4^{4/3}\psi(\chi P)^{1/3}. \tag{12}$$

The region of validity of this solution is indicated as region I in Fig. 3.

(*ii*) *Large cracks (high P)*. In the region $c \gg c^*$, Eq. (6c) applies and we have maximum microstructural interaction. The procedure to a solution is entirely the same as in the previous case, except that now T_∞ replaces T_0 in Eq. (12). Thus

$$\sigma_m^\infty = 3T_\infty^{4/3}/4^{4/3}\psi(\chi P)^{1/3} \tag{13}$$

This solution applies in region III in Fig. 3.

It is for intermediate cracks, region II in Fig. 3, that analytical solutions are difficult to obtain. Here numerical procedures will be required, but the route is nevertheless the same as before; determine $\sigma_a(c)$ from Eq. (11) in conjuction with Eq. (6b) and apply the instability condition, taking account of the increased stabilization arising from the K_μ term. To proceed this way we must first determine the values of the parameters in Eqs. (6) and (11). We address this problem in the next section.

III. DERIVATION OF T CURVE FROM INDENTATION STRENGTH DATA

A. Crack geometry and elastic/plastic contact parameters

Our first step towards a complete parametric evaluation of the $\sigma_m(P)$ data is to seek *a priori* specifications of the dimensionless quantities ψ and χ in Eq. (11). The parameter ψ is taken to be material independent, since it is strictly a crack geometry term. The parameter χ does depend on material properties, however, relating as it does competing elastic and plastic processes in the indentation contact.[13] We note that these parameters do not appear in the microstructural term K_μ in Eq. (6), so ideally we can "calibrate" them from

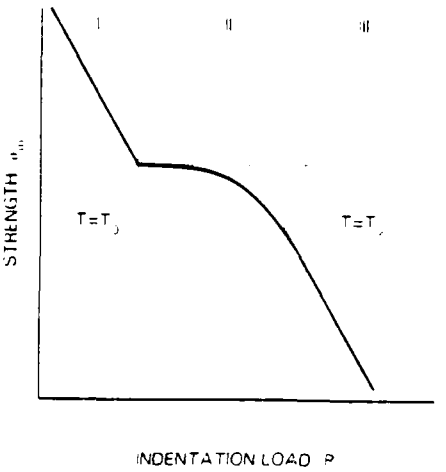

FIG. 3. Schematic strength versus indentation load plot incorporating the influence of bridging ligaments into the crack propagation response (logarithmic coordinates). The solid line represents the general solution [Eqs. (6) and (11)]. The dashed lines represent asymptotic solutions obtained analytically for small cracks [region I, Eq. (12)] and large cracks [region III, Eq. (13)].

tests on materials that do *not* exhibit T-curve behavior. The details of such calibrations are given in the Appendix. The values we use are $\psi = 1.24$ and $\gamma = 0.0040\,(E/H)^{1/2}$, where H is the hardness.

B. Bounding parameters for the regression procedure

We have indicated that solutions for region II of the strength-load response of Fig. 3 must be obtained numerically. Here we shall outline the regression procedure used to deconvolute the T curve for a given set of $\sigma_m(P)$ data.

To establish reasonable first approximations for a search/regression procedure, we note two experimental observations. The first is from the indentation/strength data of Cook *et al.*[1] In a number of materials the $\sigma_m(P)$ data tended strongly to the asymptotic limit of region III at large indentation loads (Fig. 3), reflecting the upper, steady-state toughness T_∞ [see Eq. (13)]. No analogous transition corresponding to T_0-controlled strengths in region I was observed: at low indentation loads the strength data were truncated by failures from natural flaws. Notwithstanding this latter restriction, we may use Eqs. (12) and (13) (with calibrated values of ψ and γ from Sec. III A) to set upper bounds to T_0 and lower bounds to T_∞ from strength data at the extremes of the indentation load range. We expect from the observations of Cook *et al.* that the lower bound estimate of T_∞ probably lies closer to the true value than the upper bound estimate to T_0.

The second experimental observation is from the crack propagation work of Swanson *et al.*,[5] who estimated the average distance between bridging sites at 2–5 grain diameters. We accordingly take the lower bound estimate for the interligament spacing d at 1 grain diameter. Similar bounding estimates for c^* are more difficult, although the condition $c^* > d$ must be satisfied.

There is one further parameter we have to specify, and that is the exponent of the ligament stress-extension function m. We have alluded to the fact that the observations of Swanson *et al.* indicate that a stabilizing, tail-dominated stress-separation function should be appropriate, with $m > 1$ in Eq. (5).

C. Regression procedure

With the first approximations thus determined we search for the set of parameters for each set of $\sigma_m(P)$ data. The scheme adopted to do this is as follows.

(1) The T curve is set from Eqs. (1) and (6) and the equilibrium $\sigma_c(c)$ response is calculated from Eq. (11) at each indentation load for which there are *measured* strength data.

(2) The *predicted* strength at each indentation load is determined numerically from the instability requirement $d\sigma_c/dc = 0$ (with the proviso that if more than one maximum in the $\sigma_c(c)$ function exists, it is the greater that determines the strength—see Sec. IV).

(3) The predicted strengths are compared with the corresponding measured strengths and the mean variance thereby calculated for a given set of T-curve parameters.

(4) The T-curve parameters are incremented and the calculation of the variance repeated, using a matrix search routine. The increments in the search variables were 0.05 MPa $m^{1/2}$ for the toughness parameters T_0 and T_∞ and 5 μm for the dimension parameters d and c^*.

(5) The set of T-curve parameters yielding the minimum residual variance is selected.

IV. RESULTS

The materials analyzed in this study are listed in Table I, along with their Young's modulus, hardness, grain size, and minor phase percentage. Previously published[1,3,4,11] indentation-strength data for these materials was used for the T-curve deconvolutions. [Some data were removed from the original $\sigma_m(P)$ data sets at large indentation loads, where the influence of secondary lateral cracking was suspected to have significantly decreased the magnitude of the residual stress intensity factor.[20]] The resultant parameter evaluations are given in Table II.

Our first exercise was to select a fixed value of the exponent m for the T-curve evaluations. Accordingly a preliminary analysis of the $\sigma_m(P)$ data for two materials displaying particularly strong T-curve influences in their strength responses, namely the VI1 and VI2 aluminas, was carried out. Figure 4 shows the minimum resid-

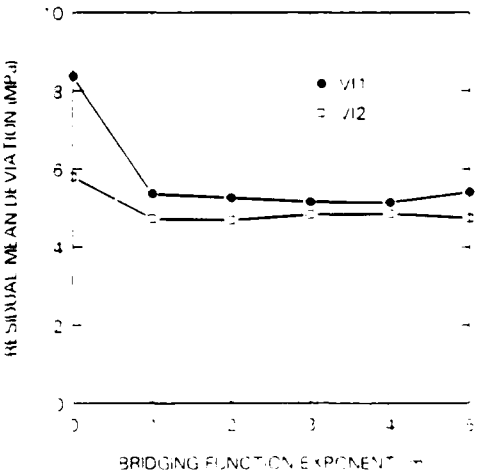

FIG. 4. The residual mean deviation between fitted and measured indentation-strength functions versus bridging function exponent m for the VI aluminas. Note the relative insensitivity for m [illegible].

ual mean deviation as a function of m for these materials. The deviation for both materials is greatest at $m = 0$ but thereafter at $m \geq 1$ is insensitive to the choice of exponent. The value somewhat arbitrarily chosen for this study was $m = 2$ in accord with that adopted in the concrete literature.[10]

To illustrate the procedure and at the same time to gain valuable insight into the crack evolution to failure let us focus now on just two of the listed alumina materials in Table I, VI2 and AD96. Figure 5 shows the strength versus indentation load data for these materials.[1] The data points in this figure represent means and standard deviations of approximately ten strength tests at each indentation load. The solid lines are the best fits [Eqs. (1), (6), and (11)] to the data. The dashed lines represent T_0- and T_∞-controlled limits [Eqs. (12) and (13)]. As can be seen, the fitted curves smoothly intersect the T_∞-controlled limit at large indentation loads, this tendency being greater for the AD96 material. This smooth connection is a reflection of our choice of m above; for $m < 2$ the $\sigma_m(P)$ curve intersects the T_∞ limit with a discontinuity in slope. At intermediate indentation loads the strengths tend to a plateau level, more strongly for the VI2 material. In line with our contention that this plateau is associated with a strong microstructural influence we might thus expect the VI2 material to exhibit a more pronounced T curve. The larger separation of the T_0- and T_∞-controlled limits for the VI2 material in Fig. 6 supports this contention. Finally, at small indentation loads the strengths cut off abruptly at the T_0-controlled limit, corresponding to the case

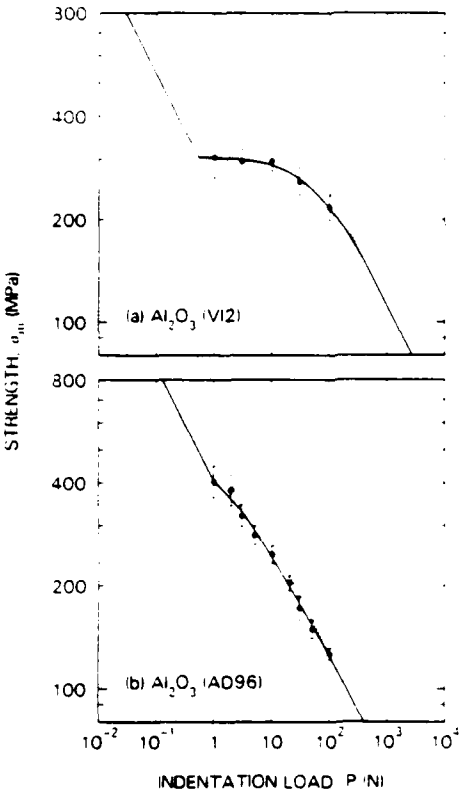

FIG. 5. Indentation-strength data fits for the VI2 and AD96 aluminas. Note the relatively pronounced plateau for the VI2 material, indicative of a strong T-curve influence. Oblique dashed lines are T_0- and T_∞-controlled limiting solutions.

TABLE I. Materials analyzed in this study

Material		Young's modulus E/GPa	Hardness H/GPa	Grain size μm	Minor phase %	Ref
Alumina	VI1	393	19.1	20	0.1	1
	VI2	393	19.0	41	0.1	1
	AD999	386	20.1	3	0.1	1
	AD96	303	14.1	11	4	1
	AD90	276	13.0	4	10	1
	F99	400	16.1	11	1	1
	HW	206	11.7	28	0.3	1
	Sapphire	425	21.8			1
Glass–ceramics	SL1	87.9	4.4	1.2	33	1,3
	SL2	87.9	4.3	1.9	22	1,3
	SL3	87.9	4.8	2.3	20	1,3
	Macor	64.1	2.0	17	50	4
	Pyroceram	108	8.4	1		4
Barium titanate	CH(cub.)	123	5.0	7		1,5
	CH(tet.)	123	5.0	7		1,5

where the crack intersects no bridges prior to unlimited instability.

Figures 6 and 7 show the corresponding equilibrium $\sigma_a(c)$ and $T(c)$ functions that underlie the curve fits in Fig. 5. The $\sigma_a(c)$ responses are plotted for several indentation loads, embracing the data range covered in the indentation-strength experiments (e.g., Fig. 5). The most distinctive feature of these curves is that at low indentation loads, where the initial crack size is somewhat smaller than the first barrier distance d, there are two maxima, most notably in the VI2 material. The first maximum, at $c < d$, is a pure manifestation of the crack stabilization due to the residual contact stress term [Eq. (11)].[19] The second maximum, at $c > d$, results from the additional, abrupt stabilization associated with the microstructural closure forces. Of the two maxima, it is the greater that determines the strength. Thus at very low P (corresponding to region I in Fig. 3) the first maximum wins, and the instability takes the crack system to failure without limit (e.g., the $P = 0.1$ N curves for both the VI2 material in Fig. 6 and the AD96 material in Fig. 7). At intermediate P (region II in Fig. 3) the second maximum becomes dominant, in which case the crack arrests before failure can ensue (e.g., the $P = 1$ N curves in Figs. 6 and 7). Note that the second maximum for the VI2 alumina occurs at $\simeq 100\,\mu$m, consistent with abrupt initial jumps of 2–5 grain diameters reported by Swanson *et al.* At large P (region III in Fig. 3) the curves tend more and more to a single pronounced maximum, as we once more enter a region of invariant toughness. In all cases, however, we note that the stabilizing influences of the residual and microstructural stress intensity factors render the strength insensitive to the intial crack length.

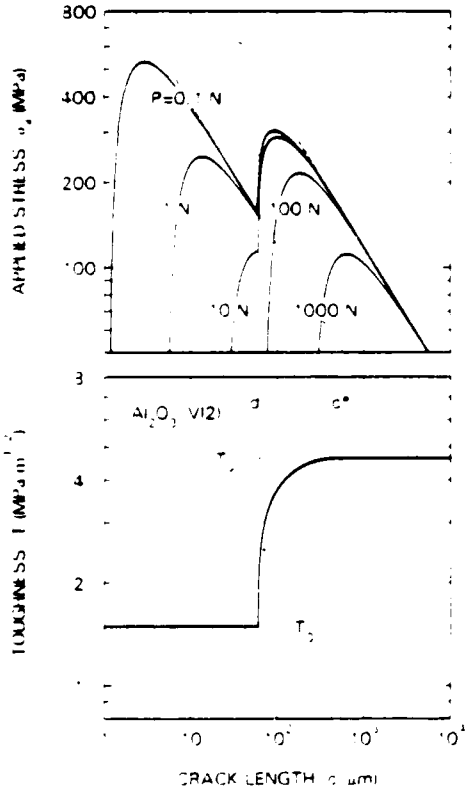

FIG. 6. (a) Applied stress versus equilibrium crack length at different indentation loads and (b) corresponding T curve, for VI2 alumina, as derived from the indentation-strength data in Fig. 5.

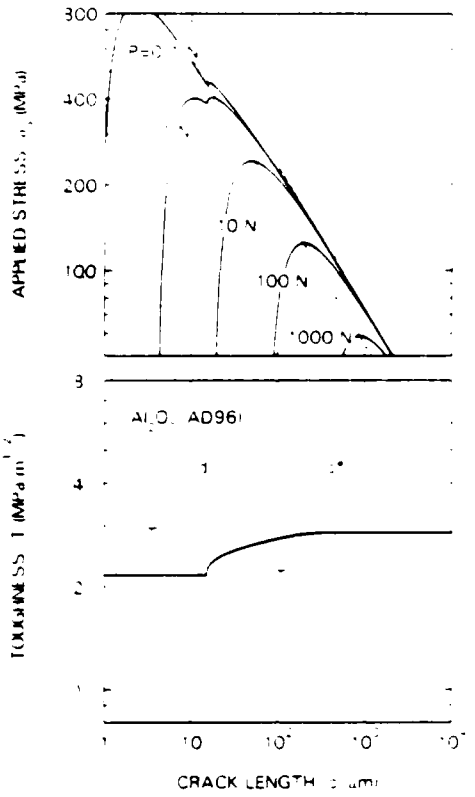

FIG. 7. (a) Applied stress versus equilibrium crack length and (b) corresponding T curve, for AD96 alumina.

It is in the transition region, region II, where the form of the T curve most strongly influences the crack stability and strength properties. The T curve for the VI2 alumina rises more steeply than that for the AD96 alumina. The difference in responses for the two materials may be seen most clearly in the $\sigma_a(c)$ curves for $P = 10$ N, Figs. 6 and 7. In VI2 alumina the restraint exerted on the crack by the interfacial bridges is apparently much stronger than in AD96. We note that the indentation-strength curves in Fig. 5 may be seen as "rotated" versions of the T curves in Figs. 6 and 7.

A word is in order here concerning the "sensitivity" of the parameter evaluation to the range of data. Figure

8 shows the deconvoluted T curves for the VI2 material with individual data points at either end of the indentation load range deliberately omitted from the base data in Fig. 5(a). When data are "lost" from the large P end, the high $T(c)$ part of the curve is most affected; similarly, for data omissions at the small P end, the low $T(c)$ part of the curve is most affected. We may regard the curve shifts in Fig. 8 as characterizing the *systematic* uncertainty in our parameter evaluations, just as the mean residual deviation in the regression procedure characterizes the *random* uncertainty. We note that it is those parameters that control the upper and lower bounds of the T curve that are subject to the greatest uncertainty, since it is in these extreme regions (especially in the T_0-controlled region) where indentation-strength data are most lacking. The central portions of the T curves in Fig. 8 are not altered substantially by the deletion of strength data.

Subject to the above considerations, we may now usefully summarize the relative T-curve behavior for the remainder of the materials listed in Table II. The T curves are shown in Figs. 9–11 for each of the material types, aluminas, glass–ceramics, and barium titanates. Special attention may be drawn to the fact that the curves for the microstructurally variant materials in each of these composite plots tend to cross each other. We note in particular that the curves for the polycrystalline aluminas in Fig. 9 cross below that for sapphire at small crack sizes, consistent with earlier conclusions that the intrinsic polycrystal toughness (T_0) is governed by grain boundary properties.[1]

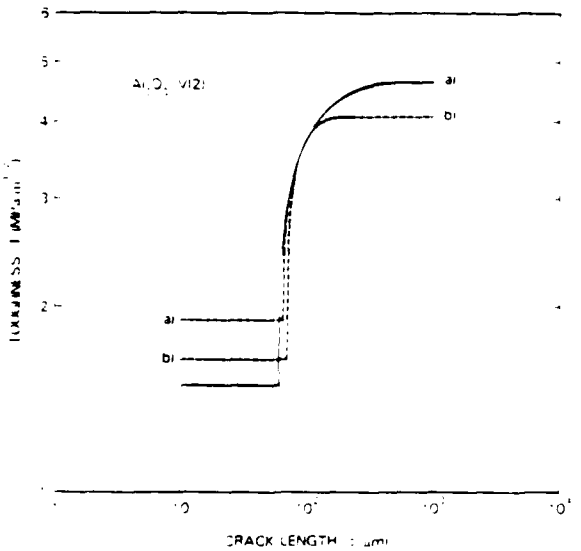

FIG. 8. Deconvoluted T-curve plots for the VI2 alumina using full indentation-strength data set from Fig. 5(a) (solid lines) and same data truncated (dashed lines) by removal of extreme data points at (a) low P and (b) high P.

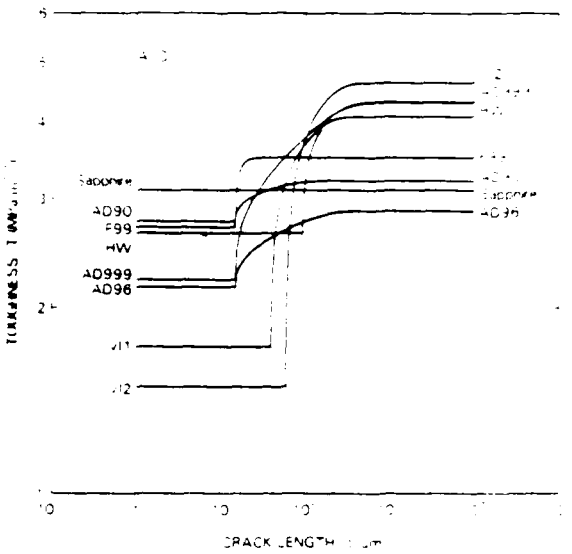

FIG. 9. Composite plot of the deconvoluted T curves for the alumina materials.

V. DISCUSSION

We have considered a fracture toughness model based on an independently verified interface restraint mechanism[3,9] for explaining the microstructural effects previously reported in indentation/strength data.[1–4] A key feature of our modeling is the strong stabilizing effect of grain-scale ligamentary bridges on the stability conditions for failure. (In this sense our explanation differs somewhat from that originally offered by us in

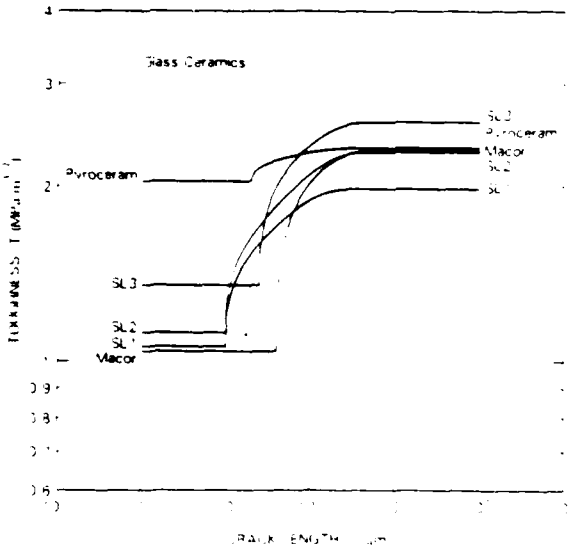

FIG. 10. Composite plot of the deconvoluted T curves for the glass–ceramic materials.

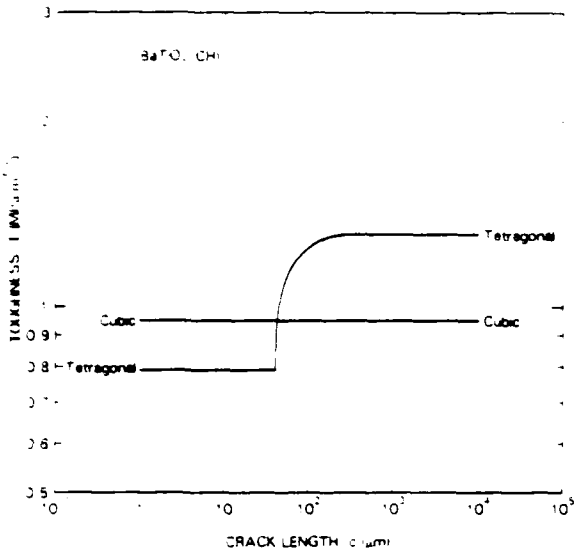

FIG. 11. Composite plot of the deconvoluted T curves for the barium titanate material.

Ref. 1, where it was tacitly suggested that the microstructural influence might be represented as a *positive decreasing* function of crack size. The distinction between negative increasing and positive decreasing K_μ functions is not easily made from strength data alone.) *Although the earlier experimental observations used to* establish the model[18] were based almost exclusively on one particular alumina ceramic,[1] our own detailed crack observations, and those of others, strongly suggest that the model is generally applicable to other nontransforming ceramics; the discontinuous primary crack traces characteristic of the bridging process have since been observed in other aluminas,[2,21] glass–ceramics,[2,21,22] SiC ceramics,[23] and polymer cements.[24] The fact that the resultant strength equations from the model can be fitted equally well to all the materials examined in the present study serves to enhance this conviction.

A characteristic feature of the failure properties of the materials with pronounced T curves (e.g., VI2 alumina) is the relative insensitivity of the strength to initial flaw size. This is a vital point in relation to structural design. Materials with strong T-curve responses have the quality of flaw tolerance. Ideally, it would seem that one should seek to optimize this quality. Associated with this tolerance is an enhanced crack stability. This offers the potential detection of failures. On the other hand, there is the indication that such benefits may only be wrought by sacrificing high strengths at small flaw sizes. This tendency is clearly observed in the way the strength curves cross each other in Figs. 7–9 in Ref. 1 (corresponding to crossovers seen here in the T curves, Figs. 9–11). In other words, the designer may have to practice the gentle art of compromise.

We reemphasize that the T-curve parameters derived from the strength data (Table II) are elements of curve fitting and are subject to systematic as well as to the usual random uncertainties. Since any four of these parameters are independent, our numerical procedure, regardless of "goodness of fit," cannot be construed as "*proof*" *of our model.* Nevertheless, we may attach strong physical significance to these parameters. For example, the relatively large values of Γ_0 and c^* for the VI materials relative to the corresponding parameters for the F99 alumina is a clear measure of a greater T-curve effect in the former. More generally, the aluminas with

TABLE II. T-curve parameters derived from strength data for m = 2 (from Refs. 1, 3, 4, 11).

Material	T_0 MPa m$^{1/2}$	T_∞ MPa m$^{1/2}$	Γ_0 (J m^{-2})	Γ_∞ (J m^{-2})	d (μm)	c^* (μm)	σ^* MPa	x^* (μm)
VI1	1.73	4.08	3.8	10.4	40	420	280	0.11
VI2	1.49	4.63	2.8	11.8	60	540	328	0.11
AD999	2.22	4.30	6.4	12.0	15	715	158	0.19
AD96	2.16	2.87	8.5	5.6	15	460	80	0.19
AD90	2.76	3.21	15.8	4.6	15	210	75	0.18
F99	2.70	3.50	9.1	5.4	15	30	405	0.04
HW	2.64	4.31	16.9	21.4	95	710	153	0.42
Sapphire	3.10	3.10	11.3	0				
SL1	1.06	1.98	6.4	11.2	10	335	122	0.27
SL2	1.12	2.29	7.1	15.0	10	485	129	0.35
SL3	1.35	2.58	10.4	19.0	25	505	133	0.43
Macor	1.04	2.30	8.4	20.4	40	535	132	0.46
Pyroceram	2.04	2.33	19.3	5.4	20	415	35	0.48
CH(cub)	1.95	1.95	3.7	0				
CH(tet)	0.79	1.35	2.5	3.6	40	330	70	0.14

glassy phases at their grain boundaries,[24] or with smaller grain size (Tables I and II) have relatively low toughness indices, $\Gamma \sim \Gamma_0$, indicating that there is some kind of trade-off between macroscopic and microscopic toughness levels, and that this trade-off is controlled by the microstructure. We note also that the maximum stress-separation range parameters u^* for the materials are in the range 0.1–0.4 μm, consistent with crack opening displacement observations at the bridging sites.[9,12,21–23] We thus suggest that such parameters could serve as useful guides to materials processors, for tailoring materials with desirable, predetermined properties, especially with regard to grain boundary structure.

Mention was made in Sec. IV of the sensitivity of the parameter evaluations to the available data range. This has implications concerning conventional, large-crack toughness measurements. To investigate this point further we plot in Fig. 12 the T_∞ values determined here against those measured independently by macroscopic techniques. The degree of correlation in this plot would appear to lend some confidence to our fitting procedure (and to our *a priori* choices for the parameters ψ and γ). Since most of our strength data tend to come from regions toward the top of the T curve we should perhaps not be too surprised at this correlation.

Finally, we may briefly address the issue of test specimen geometry in connection with the accuracy of the parameter evaluations. It has been argued elsewhere[9] that test specimen geometry can be a crucial factor in the T-curve determination. It might be argued, for instance, that "superior" parameter evaluations could be obtained from larger crack geometries, particularly the c^*, T_∞ parameters. However, the indentation methodology takes us closer to the strengths of specimens with natural flaws, in particular to the T-controlled regions (notwithstanding our qualifying statements earlier concerning this parameter), so that the present evaluations may be more appropriate for designers.

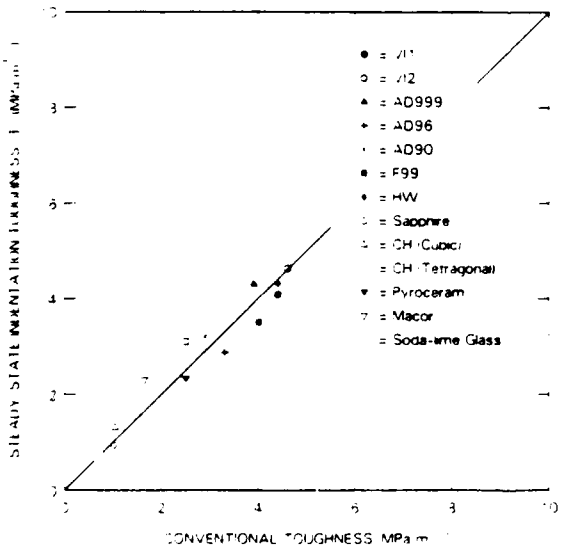

FIG. 12. Plot of T_∞ (Table II) as a function of independently measured toughness using conventional macroscopic specimens.

VI. CONCLUSIONS

(1) An independently confirmed ligament bridging model is used as the basis for analyzing observed indentation-strength data for a wide range of polycrystalline ceramic materials.

(2) Those materials with pronounced T curves show the qualities of "flaw tolerance" and enhanced crack stability.

(3) A fracture mechanics treatment of the indentation fracture system with microstructure-associated factors incorporated allows for the (numerical) deconvolution of toughness/crack-length (T-curve) functions from these data.

(4) Comparisons within a range of aluminas suggest that those materials with "glassy" grain boundaries and smaller grain size have less pronounced T curves than those with "clean" boundaries.

(5) The indentation-strength technique and the toughness parameters deriving from it should serve as useful tools for the development of ceramic materials with predetermined properties, especially with respect to grain boundary structure and chemistry.

ACKNOWLEDGMENTS

The authors thank C. Thompson for assistance with some of the computer programs used in this work.

Funding for the National Bureau of Standards component of this work was provided by the Air Force Office of Scientific Research.

APPENDIX: EVALUATION OF ψ AND γ

Here we derive numerical values for the dimensionless parameters ψ and γ characterizing the crack geometry and the intensity of the residual contact stress, respectively. The choices for these should yield agreement between measured strength and toughness properties of homogeneous materials with no measurable T-curve behavior (i.e., $K_\mu = 0$, $T = T_0 = T_\infty$).

We begin with the geometrical ψ term, which is assumed to be material independent. From the applied stress (strength) σ_m and crack length c_m at the instability point of an indentation, we can show that[5]

$$\psi = 3T_0 / (\sigma_m c_m^{1/2}). \qquad \text{A1}$$

Measurements of $\sigma_m c_m^{1/2}$ for several homogeneous mate-

rials confirm that Eq. (A1) describes the toughness-instability properties[25,26] for $\psi = 1.24$. We note that this is very close to the value of 1.27 calculated by finite element analyses of semicircular cracks in surfaces of bend specimens.[27]

For the χ term we turn to Ref. 13, where it is shown that

$$\chi = \xi(E/H)^{1/2}, \tag{A2}$$

where ξ is a material-independent constant. With this result Eq. (12) may be rewritten as[28]

$$T_i = \eta(E/H)^{1/8}(\sigma_m^2 P^{1/3})^{3/4}, \tag{A3}$$

where

$$\eta = (256\psi^{1/3}\xi^{-27})^{1/4} \tag{A4}$$

is another material-independent constant. From measurements of $\sigma_m^2 P^{1/3}$ for a similar range of homogeneous material we obtain $\eta = 0.52$.[26] Hence eliminating ξ from Eqs. (A2) and (A4) yields

$$\chi = 27\eta^4(E/H)^{1/2}/256\psi^2, \tag{A5}$$

which gives $\chi = 0.0040(E/H)^{1/2}$.

REFERENCES

R. F. Cook, B. R. Lawn, and C. J. Fairbanks, J. Am. Ceram. Soc. **68**, 604 (1985).

R. F. Cook, B. R. Lawn, and C. J. Fairbanks, J. Am. Ceram. Soc. **68**, 616 (1985).

R. F. Cook, S. W. Freiman, and T. L. Baker, Mater. Sci. Eng. **77**, 199 (1986).

C. J. Fairbanks, B. R. Lawn, R. F. Cook, and Y. W. Mai, in *Fracture Mechanics of Ceramics*, edited by R. C. Bradt, A. G. Evans, D. P. H. Hasselman, and F. F. Lange (Plenum, New York, 1986), pp. 23–35.

H. Hübner and W. Jillek, J. Mater. Sci. **12**, [illegible]

R. Knehans and R. Steinbrech, J. Mater. Sci. Lett. **1**, [illegible]

R. Steinbrech, R. Knehans, and W. Schaarwächter, J. Mater. Sci. **18**, 265 (1983).

P. L. Swanson, C. J. Fairbanks, B. R. Lawn, Y.-W. Mai, and B. R. Hockey, J. Am. Ceram. Soc. **70**, 279 (1987).

Y.-W. Mai and B. R. Lawn, Annu. Rev. Mater. Sci. **16**, 415 (1986).

Y.-W. Mai and B. R. Lawn, J. Am. Ceram. Soc. **70**, 289 (1987).

R. F. Cook, S. W. Freiman, B. R. Lawn, and R. C. Pohanka, Ferroelectrics **50**, 267 (1983).

P. L. Swanson, in *Advances in Ceramics*, in press.

B. R. Lawn, A. G. Evans, and D. B. Marshall, J. Am. Ceram. Soc. **63**, 574 (1980).

D. R. Clarke, B. R. Lawn, and D. H. Roach, in Ref. 4, pp. 341–350.

I. N. Sneddon, Proc. R. Soc. London Ser. A **187**, 229 (1946).

B. R. Lawn and T. R. Wilshaw, *Fracture of Brittle Solids* (Cambridge U. P., Cambridge, 1975).

D. B. Marshall, B. N. Cox, and A. G. Evans, Acta Metall. **33**, 2013 (1985).

D. B. Marshall and B. R. Lawn, J. Mater. Sci. **14**, 2001 (1979).

D. B. Marshall, B. R. Lawn, and P. Chantikul, J. Mater. Sci. **14**, 2225 (1979).

R. F. Cook and D. H. Roach, J. Mater. Res. **1**, 589 (1986).

R. F. Cook (unpublished work).

K. T. Faber and A. G. Evans, Acta Metall. **31**, 577 (1983).

K. T. Faber and A. G. Evans, J. Am. Ceram. Soc. **66**, C-94 (1983).

S. L. Fortner (unpublished work).

R. F. Cook and B. R. Lawn, J. Am. Ceram. Soc. **66**, C-200 (1983).

R. F. Cook, Ph.D. thesis, University of New South Wales, Australia, 1985.

J. C. Newman and I. S. Raju, Eng. Fract. Mech. **15**, 185 (1981).

P. Chantikul, G. Anstis, B. R. Lawn, and D. B. Marshall, J. Am. Ceram. Soc. **64**, 539 (1981).

Reprinted from the Journal of the American Ceramic Society, Vol. 70, No. 6, June 1987
Copyright by The American Ceramic Society, Inc.

Microstructural Effects on Grinding of Alumina and Glass-Ceramics

DAVID B. MARSHALL*
Rockwell International Science Center, Thousand Oaks, California 91360

BRIAN R. LAWN*
Ceramics Division, National Bureau of Standards, Gaithersburg, Maryland 20899

ROBERT F. COOK*
I.B.M., Thomas J. Watson Research Center, Yorktown Heights, New York 10598

Grinding forces were measured in aluminas and glass-ceramics with various microstructures. The microstructures were found to exert a profound influence on the machinability. In particular, the controlling toughness variable is that which pertains to small cracks, not that conventionally measured in a large-scale fracture specimen.

It is well documented that the principal material variable in microfracture-controlled properties of brittle ceramics, such as erosion, wear, and machining, is the "toughness."[1] This is in accord with intuition: the greater the resistance to fracture, the harder it should be to remove material in localized, cumulative, surface contact processes. Implicit in existing material removal theories is the presumption that toughness is a single-valued quantity for a given material. Recent studies of the fracture properties of a wide range of ceramics call this presumption into serious question; toughness is generally *not* a material constant, but rather some increasing function of crack size (*R* curve, or *T* curve).[2] In certain aluminas, for example, the toughness can increase by a factor of 3 or so, depending on the microstructure.[3,4] The *T*-curve effect is seen most strongly in aluminas with larger grain sizes and lower contents of grain-boundary glassy phase. Most notably, the *T* curves for different aluminas tend to cross each other,[4] so that the toughness rankings at large and small crack sizes appear to be reversed. Clearly, if we wish to retain toughness as an indicator of wear resistance, we need to qualify the scale on which this parameter is determined. Indeed, such a need was foreshadowed in an earlier experimental study on the erosion resistance of ceramic materials by Wiederhorn and Hockey.[5]

Accordingly, surface grinding tests were made on selected ceramic materials for which well-characterized *T*-curve data are available. The primary materials were aluminas from a previous study,[4] where the resistance characteristics were determined from the strengths of specimens containing indentation flaws.[6] In addition, two commercial glass-ceramics were tested. A subsequent quantitative analysis of the indentation-strength data has provided upper (large crack size) and lower (small crack size) bounds, T_∞ and T_0, to the *T* curves for these materials.[7] Table I lists these parameters for comparison with the grinding results.

The grinding forces were measured using a dynamometer on the table of a surface grinding machine. Runs were made at fixed depths of cut, 5, 10, 15, and 20 μm, using a 240-grit diamond wheel (width 10 mm), rotating at 3300 rpm with a horizontal feed rate of 16 mm·s^{-1} and with water-soluble oil lubrication. The conditions of our experiments were such that the scale of individual damage events was always much smaller than the depths of cut. The specimens were first cut into bars 5 mm wide and then mounted in a row on the dynamometer so that force measurements could be made on all materials in a single pass. The results are plotted in Fig. 1. Note from the relative positions of the curves that the aluminas and glass-ceramics have been ranked in order of diminishing grinding resistance in Table I.

It is immediately apparent from Fig. 1 that different aluminas and different glass-ceramics can vary widely in their grinding resistance. Thus the alumina with the highest resistance in Table I (i.e., AD90) is that with the greatest glass content. This result may come as no surprise to those who prepare ceramic powders by ball milling: alumina spheres with high glass content are found to be far more durable than similar high-purity spheres.[8] Note also from Table I that for aluminas of comparable purity those with higher grinding resistance have finer grain sizes (cf. AD999 and Vistal). Most interesting, however, is the quantitative correlation between grinding resistance and toughness parameters. The macroscopic toughness T_∞ (i.e., the toughness K_{Ic} we measure in conventional large-scale fracture tests) actually shows an *inverse* correlation with the grinding resistance. On the other hand, the microscopic toughness T_0 does appear to scale in the right direction. The implication here, of course, is that the grinding damage process is determined at the scale of the microstructure. The data for the two glass-ceramics in Table I serve to reinforce the point: on the basis of the T_∞ values we would be unable to choose between the two materials, whereas the relative values of T_0 confirm Macor (specified as a machinable glass-ceramic by its manufacturer) as the material of lower grinding resistance.

We conclude, therefore, that the time-honored conception of "toughness" as a universal indicator of superior mechanical properties, at least on the microscale, needs to be carefully qualified. The use of conventional fracture toughness evaluations to predict resistance to wear, erosion, and machining may lead to imprudent choices of materials for structural applications. On the positive side, a more complete understanding of the micromechanics that determine the complete crack resistance curve may ultimately help us optimize microstructural elements (glass content, grain size, etc.) for minimum surface degradation.

Table I. Comparison of Toughness and Grinding Resistance Parameters*

Material		Additive (%)	Grain size (μm)	T_∞ (MPa·m$^{1/2}$)	T_0 (MPa·m$^{1/2}$)
Alumina	AD90	10	4	3.2	2.8
	Sapphire			3.2	3.1
	AD96	4	11	2.9	2.2
	AD999	0.1	3	4.3	3.5
	Vistal I	0.1	20	4.1	1.7
	Vistal II	0.1	40	4.6	1.5
Glass-ceramic	Pyroceram[†]		1.5	2.3	2.0
	Macor[‡]		13	2.3	1.0

*T_∞ and T_0 evaluated from indentation-strength data (Ref. 5). Material rankings in order of decreasing resistance (from Fig. 1). [†]Coors Porcelain Co., Golden, CO. [‡]Adolf Meller Co., Providence, RI. [§]Corning Glass Co., Corning, NY.

CONTRIBUTING EDITOR — T. MICHALSKE

Received October 9, 1986; revised copy received December 5, 1986; approved December 22, 1986.

Supported by the Rockwell Independent Research and Development Program (DBM) and the U.S. Army Research Office (BRL).

*Member, the American Ceramic Society.

*Only those materials originally available in disk form in that earlier work were selected. The strength data for these specimens are not limited by edge failures, so the resistance characteristics are more likely to reflect the intrinsic microstructural influence (Ref. 4).

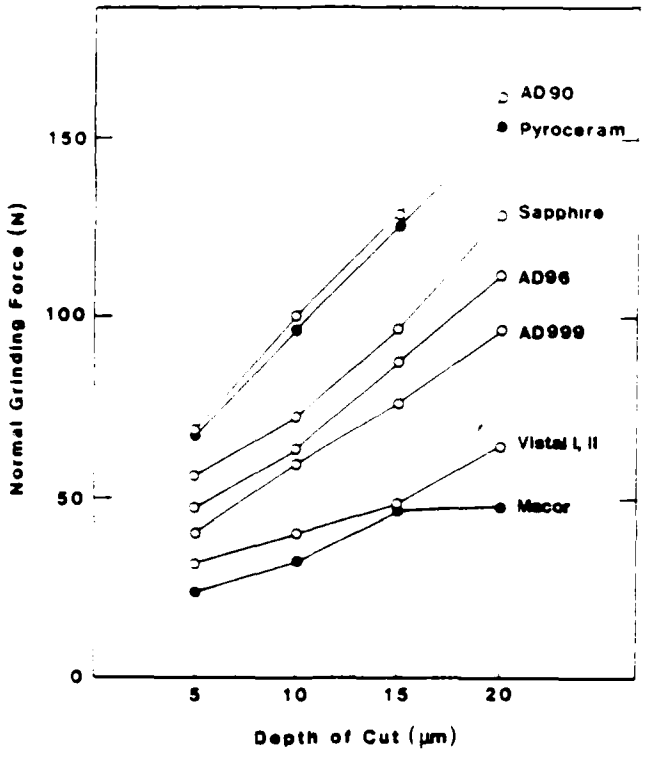

Fig. 1 Vertical grinding forces as function of depth of cut. Open symbols represent aluminas; closed symbols represent glass ceramics.

REFERENCES

A. W. Ruff and S. M. Wiederhorn, Ch. 2 in Treatise on Materials Science and Technology, Vol. 16, Edited by C. M. Preece, Academic, New York, 1979.

Y. W. Mai and B. R. Lawn, "Crack Stability and Toughness Characteristics in Brittle Materials," *Ann. Rev. Mater. Sci.*, **16**, 415–39 (1986).

R. Knehans and R. Steinbrech, "Memory Effect of Crack Resistance During Slow Crack Growth in Notched Alumina Specimens," *J. Mater. Sci. Lett.*, **1** [8] 327–29 (1982).

[4]R. F. Cook, B. R. Lawn, and C. J. Fairbanks, "Microstructure-Strength Properties in Ceramics. I. Effect of Crack Size on Toughness," *J. Am. Ceram. Soc.*, **68** [11] 604–15 (1985).

[5]S. M. Wiederhorn and B. J. Hockey, "Effect of Material Parameters on the Erosion Resistance of Brittle Materials," *J. Mater. Sci.*, **18** [3] 766–80 (1983).

[6]R. F. Cook, C. J. Fairbanks, B. R. Lawn, and Y.-W. Mai, to be published in *J. Mater. Res.*

[7]F. F. Lange, private communication.

END

DATE

FILMED

DTIC

4/88